BNWL-264

AEC RESEARCH and DEVELOPMENT REPORT

PRELIMINARY HYDRAULIC ANALYSIS OF THE CONCEPTUAL FFTF CERMET DRIVER FUEL ELEMENT DESIGN

G. J. CRANDALL

JULY 1966

BATTELLE-NORTHWEST
BATTELLE MEMORIAL INSTITUTE / PACIFIC NORTHWEST LABORATORY

LEGAL NOTICE

PACIFIC NORTHWEST LABORATORY
RICHLAND, WASHINGTON
operated by
BATTELLE MEMORIAL INSTITUTE
for the
UNITED STATES ATOMIC ENERGY COMMISSION UNDER CONTRACT AT(45-1)-1830

PRINTED BY/FOR THE U. S. ATOMIC ENERGY COMMISSION

DISTRIBUTION

No. of Copies	
25	Atomic Energy Commission, Washington Division of Reactor Development Technology J. J. Morabito
330	Division of Technical Information Extension
47	Division of Technical Information Extension UK/U.S. Fast Reactor Exchange (12) EURATOM/U.S. Fast Reactor Exchange (35)
6	Douglas United Nuclear, Inc. C. L. Abel J. T. Baker W. A. Crossman T. C. Hall M. M. McCartney (2)
2	General Atomic Division D. Coburn
1	General Electric Company, Pleasanton L. Wilkinson
4	General Electric Company, Richland D. W. Curtiss C. Gibbons J. C. Larrew GE File Copy
4	General Electric Company, San Jose Advanced Products Operation J. H. Field
1	Isochem Inc. R. E. Olson
4	Richland Operations Office L. R. Lucas (2) R. K. Sharp Technical Information Library

No. of Copies

1 University of California, Livermore

James Hadley

37 Battelle-Northwest

D. T. Aase
F. W. Albaugh
E. R. Astley
J. M. Batch
W. A. Burns
P. D. Cohn
R. F. Corlett
G. J. Crandall
G. M. Dalen
J. M. Davidson
D. R. Doman
R. V. Dulin
L. M. Finch
C. D. Flowers
G. L. Fox
F. C. Fox
H. Harty
R. J. Hennig
D. L. Hovorka
M. T. Jakub
L. W. Lang
W. B. McDonald
K. R. Merckx
L. T. Pedersen
R. E. Peterson
W. E. Roake
D. E. Simpson
K. G. Toyoda
J. M. Yatabe
F. R. Zaloudek
Technical Information Files (5)
Technical Publications (2)

BNWL-264
UC-80, Reactor Technology

PRELIMINARY HYDRAULIC ANALYSIS OF THE CONCEPTUAL FFTF CERMET DRIVER FUEL ELEMENT DESIGN

By
G. J. Crandall
Development and Technology Engineering Section
FFTF Project

July 1966

PACIFIC NORTHWEST LABORATORY
RICHLAND, WASHINGTON

Printed in USA. Price $3.00. Available from the
Clearinghouse for Federal Scientific and Technical Information,
National Bureau of Standards, U. S. Department of Commerce,
Springfield, Virginia

TABLE OF CONTENTS

TABLE OF CONTENTS

INTRODUCTION

An analytical investigation of the hydraulic parameters and characteristics of the Fast Flux Test Facility (FFTF) driver fuel elements is essential to achieve an optimum fuel design. This study is concerned with the cermet driver fuel element as shown in BNWL-CC-175, Volume 3. The fuel element consists of a fuel rod bundle surrounded by a stainless steel liner. Fuel rod bundle and liner slip as a unit into the fuel element process tube. Spiral ribs are attached to the fuel element liner, and they create a spiral channel annulus between the fuel element liner and process tube as depicted in Figures 1 and 2.

Pressure loss is the most important hydraulic parameter of the fuel rod bundle. The reason for this is that present pump technology is such that fuel element pressure loss should be no more than 80 psi, and preferably 60 psi. The two main causes of fuel element pressure loss are the fuel rod spacers and skin friction in the fuel rod bundle. Conceptual fuel rod spacer design consists of a hexagonal honeycomb grid spacer, as illustrated in Figure 2. As shown, each pin is surrounded by four sides of a hex on one plane and four sides of a hex on a plane below and adjacent to the first.

Due to the fuel rod spacer geometry, fuel rod spacer pressure loss is difficult to predict; therefore, it is bracketed by three techniques which will be called the de Stordeur, triangular cell, and rectangular cell methods. The de Stordeur method employs an emperical equation that includes an experimentally determined drag coefficient. Both the triangular and rectangular cell methods use the Darcy-Weisbach equation for pressure loss which contains a friction factor term. The friction factors used were determined experimentally and were for flow through geometries similar to those in question.

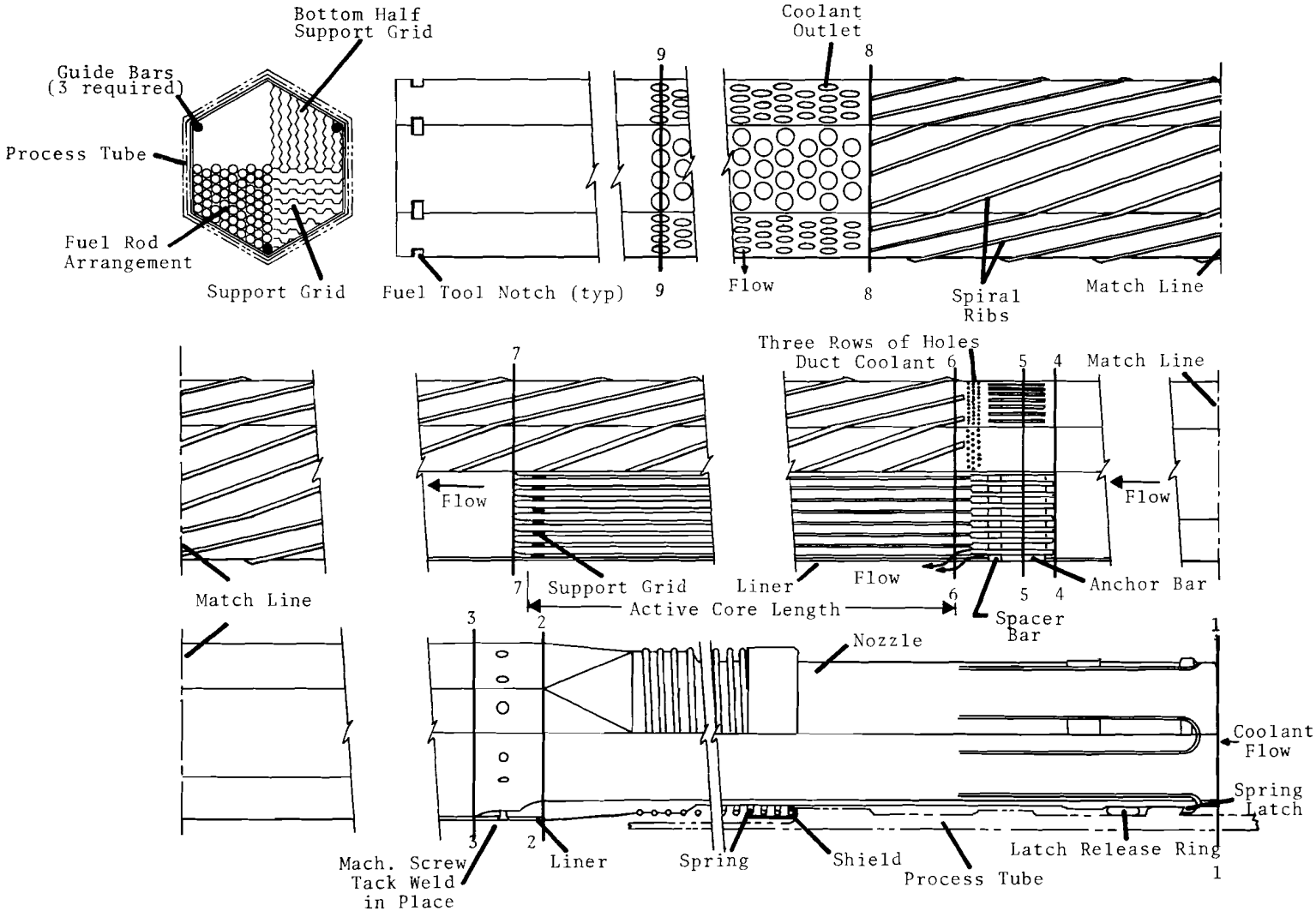

FIGURE 1. Driver Fuel Element

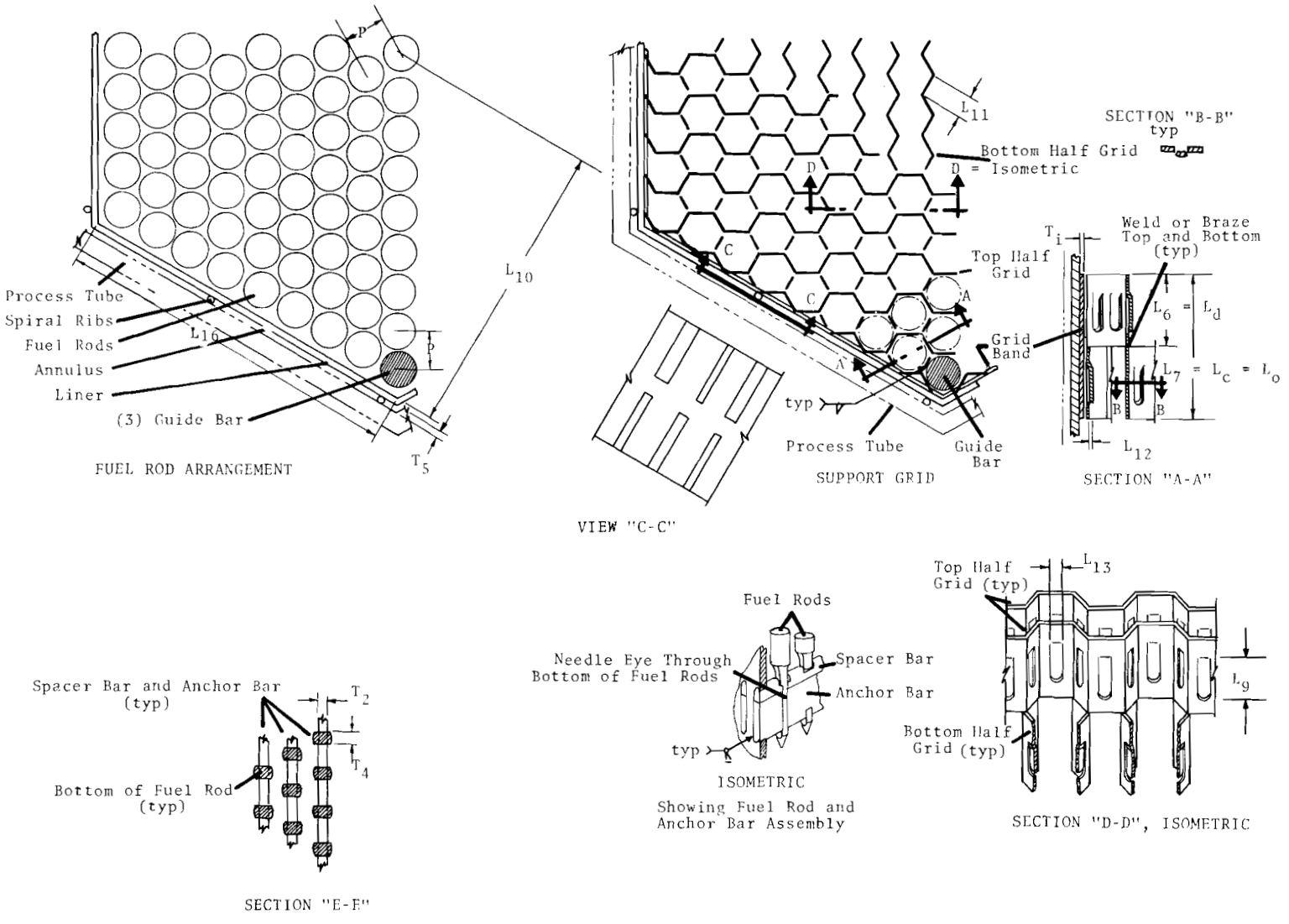

FIGURE 2. Driver Fuel Element Cross Section

Sodium flow rate through the annulus spiral channels is the most important hydraulic parameter of the fuel element annulus, since this flow will tend to flatten the temperature gradient across a fuel element. For a given annulus length, the annulus hydraulic parameters that effect this flow rate are annulus pressure loss, channel spiral angle, and channel hydraulic diameter.

The fuel rod bundle hydraulic analysis includes interaction and variation of fuel element pressure loss with all parameters except the number of fuel rods, their diameter, and length (which will be included in later studies). Interaction and variation of all important parameters including annulus pressure loss, channel spiral angle, channel hydraulic diameter, and sodium velocity are considered in the hydraulic investigation of the fuel element annulus.

Sodium leakage between annulus spiral channels and the strength of fuel rod spacer strips to withstand the fluid forces were analyzed to determine if either will be a problem.

Results of this study pertain to the fuel element conceptual design as illustrated in BNWL-CC-175, Volume 3, unless modifications are indicated. The Nomenclature and Dimensional Assumptions are defined on pages 45 through 60. Throughout this study it is assumed that liquid sodium behaves hydraulically as does the class of fluids which includes water.

SUMMARY AND CONCLUSIONS

Applying the equations presented in this study for determining fuel element pressure loss as a function of fuel rod bundle hydraulic parameters, it was found that for the required fuel element mass flow rate of 57 lb/sec, fuel element pressure loss is 129 psi ± 15%. This is 49 psi ± 40% above a maximum design value of 80 psi. The corresponding pressure difference across the fuel element liner is 36 psi maximum. Fuel rod spacers are responsible for a large percentage (62%) of the fuel element pressure loss. The following changes can reduce this component by 10, 4, and 24%, respectively.

- Removing one set of spacers
- Using elastic support dimples instead of fingers
- Decreasing the thickness of fuel rod spacer material (0.015 to 0.010 in.).

Pressure difference across the fuel element liner can be decreased to 7 psi by drilling holes in the liner at the downstream end of the fuel rods. Consequently, sodium flow rate through the annulus can be increased.

The equation developed in this study for determining sodium flow rate through the annulus as a function of annulus hydraulic parameters predicts that for a sodium flow rate of 6.7 lb/sec, annulus pressure loss is 70 psi ± 10%, and sodium leakage between channels is negligible. Skin friction in the annulus spiral channels is responsible for 84% of the annulus pressure loss.

An investigation of the variation and interaction of annulus hydraulic parameters relative to a channel hydraulic diameter of 0.091 in. indicates that decrease in annulus pressure loss with an increase in channel

spiral angle is more pronounced at higher sodium velocities and smaller spiral angles. For a spiral angle of 67 degrees, reduction of annulus pressure loss with an increase in channel hydraulic diameter is more pronounced at higher sodium velocities and smaller channel hydraulic diameters. For a hydraulic diameter of 0.091 in. and various annulus pressure losses, annulus sodium flow rate increases rapidly with an increase in spiral angle at small angles, but this method of varying flow rate becomes less effective as the angle is increased. The parameter that appears to have the greatest effect on sodium flow rate through the annulus is the spiral channel hydraulic diameter (for a given annulus length, L_3 = 4.3 ft).

This study indicates that fuel rod spacer thickness can be less than 0.015 in. and still withstand the fluid forces. However, this does not take into consideration such factors as required fuel rod support force, cyclic loading of support fingers as a result of vibration, deterioration of metal properties due to irradiation, etc.

Therefore, it can be concluded:

- Pressure loss for sodium flow through the conceptual driver fuel element design is high. Present pump technology is such that a costly and lengthy development program would be required to build pumps capable of supplying this pressure plus the other pressures required throughout the FFTF heat removal system.
- Since the fuel rod spacers are responsible for 62% of the fuel element pressure loss, redesign or design modifications of the spacers will be necessary to eliminate the problem of high fuel element pressure loss.

- Sodium flow rate through the spiral channel annulus can be varied by changing the annulus hydraulic parameters. The parameter that appears to have the greatest effect on this flow rate is the spiral channel hydraulic diameter (for a given annulus length).
- Sodium leakage between annulus spiral channels is insignificant.
- Strength of the fuel rod spacers to withstand fluid forces is sufficient.

ANALYSIS

FUEL ROD BUNDLE HYDRAULICS

This study includes sodium flow in the fuel element but not in the annulus between positions 1-1 and 9-9. Position numbers mentioned in the text refer to lines on the fuel element as illustrated in Figure 1.

General Pressure Loss Equation

The general equation defining total fuel element pressure loss is:

$$\Delta P_{fuel} = \Delta P_1 + \Delta P_{1-2} + \Delta P_{2-3} + \Delta P_{3-4} + \Delta P_5 + \Delta P_{4-6} + \Delta P_{6-7} + \Delta P_{6'-7'} + \Delta P_7 + \Delta P_{7-9} + \Delta P_9 + \Delta P_{1-9}$$

Pressure loss Δp_1 is due to entrance effects that occur as sodium enters the fuel element at position 1-1.

$$\Delta P_1 = \frac{K_1 V_1^2 \rho}{2g}$$

Entrance loss coefficient K_1 is 0.70 [2]. This value is for a sharp-edged entrance as shown in Figure 3.

Pressure losses ΔP_{1-2}, ΔP_{3-4}, and ΔP_{7-9} are due to skin friction in the fuel element between the positions indicated by the subscripts.

$$\Delta P_{1-2} = \frac{f_1 L_1 V_1^2 \rho}{D_{H_1} 2g}$$

$$\Delta P_{3-4} = \frac{f_2 L_2 V_2^2 \rho}{D_{H_2} 2g}$$

$$\Delta P_{7-9} = \frac{f_3 L_3 V_6^2 \rho}{D_{H_3} 2g}$$

Average Moody friction factors f_1, f_2, and f_3 are:

$$f = \frac{0.184}{R^{0.2}}$$

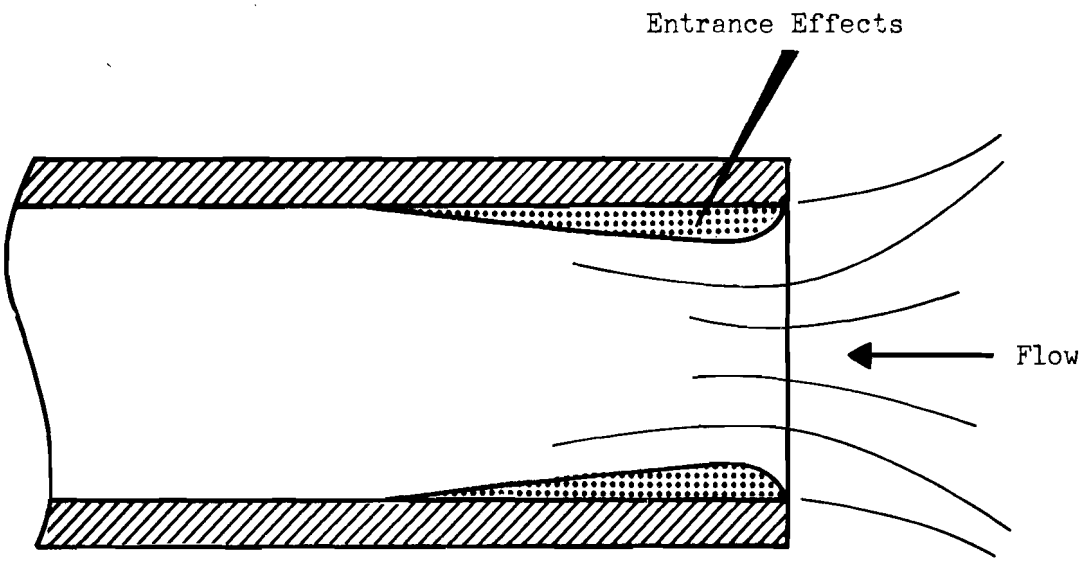

FIGURE 3. Sharp Edged Entrance

Pressure loss Δp_{2-3} is due to the nozzle between positions 2-2 and 3-3.

$$\Delta p_{2-3} = \frac{K_2(V_1 - V_2)^2\rho}{2g}$$

Nozzle loss coefficient K_2 is 0.17 [3]. It is located by knowing the nozzle expansion angle (θ) and the hydraulic diameter ratio D_{H_2}/D_{H_1}.

Pressure loss Δp_5 is due to the fuel rod anchor and spacer bars at position 5-5.

$$\Delta p_5 = \frac{\Delta p_{6-7}}{n_2}$$

This loss is difficult to predict accurately because of fluid boundary layer disturbance at position 4-4. After considering anchor and spacer bar, and rod spacer geometries, it was decided that a good approximation of bar pressure loss would be to assume that it is equal to one fuel rod spacer*. This approximation is estimated to be accurate within $\pm$ 25%.

Pressure loss Δp_{4-6} is due to entrance effects that occur as sodium enters the fuel rod bundle between positions 4-4 and 6-6.

$$\Delta p_{4-6} = \frac{K_3 V_5^2 \rho}{2g}$$

The flow area change between positions 4-4 and 6-6 is not abrupt. Sodium must flow through a length of fuel rod bundle and the fuel rod anchor and spacer bars between these positions. However, a loss coefficient for an abrupt area change ($K_3 = 0.26$) [5] is used, and it is estimated to be accurate within $\pm$ 50%.

Two values are required to locate K_3. First is σ_1, which is equal to the area ratio A_2/A_5, and second is the Reynolds number. For this case σ_1 is equal to 0.36, and an entrance loss line for a Reynolds number of infinity is used since the Reynolds number is relatively high.

*without fuel rod support fingers

Pressure loss Δp_{6-7} is due to the fuel rod spacers as depicted in Figure 2. Because of uncertainty in determining this loss, it is bracketed by the methods indicated below.

$$\Delta P_{6-7} = \frac{n_2 C_s V_s^2 A_{p_s} \rho}{A_5 \, 2g} \quad (4) \qquad \text{(de Stordeur)}$$

$$\Delta P_{6-7} = \frac{n_2 n_5 f_c L_c V_c^2 \rho 4}{D_{H_c} \, 2g} + \frac{n_2 (K_4 + K_5) V_c^2 \rho}{2g} \qquad \text{(triangular cell)}$$

$$\Delta P_{6-7} = \frac{n_2 n_5 f_o L_o V_o^2 \rho 4}{D_{H_o} \, 2g} + \frac{n_2 (K_6 + K_7) V_o^2 \rho}{2g} \qquad \text{(rectangular cell)}$$

Three problems complicate the effort to adapt the de Stordeur method to the prediction of this pressure loss. First is the determination of the spacer projected frontal area, A_{p_s}. In this study it is assumed to be the projected area of a fuel rod spacer as it would appear when looking down the fuel element.

The second problem is in obtaining a value for the fuel rod spacer drag coefficient, C_s. A figure in Reference 4 gives drag coefficients for various Reynolds numbers and types of fuel rod spacers, but coefficients are not given for the split-level, hexagonal honeycomb type of spacer with which this analysis is concerned. For lack of a better value, a coefficient for a square honeycomb spacer is used because its geometry is as close to that of a hexagonal spacer as is given in the reference even though all sides of the square spacer are on one plane while sides of the hexagonal spacer are on two planes as shown in Figure 2. For a Reynolds number ($R_s = 1.38 \times 10^4$) based on T_1, the frontal dimension of strips forming the fuel rod spacers (spacer strips), the drag coefficient for a square honeycomb spacer is $1.8^{(4)}$. This approximation of spacer drag coefficient is estimated to be accurate within $\pm$ 40%.

Problem number three is determining sodium velocity within a fuel rod spacer, V_s. As stated in Reference 4, the actual velocity in a central spacer flow cell should be used. However, peripheral and central flow cell geometries will be nearly the same if the spacer region is divided into cells as depicted in Figure 6. Therefore, average sodium velocity in a spacer is substituted for the velocity within a central spacer flow cell since they are approximately equal.

This method of accounting for fuel rod spacer pressure loss includes: an entrance and exit loss for each spacer, and it allows for fuel rod support dimples. Fluid mixing within the spacers is not considered. Accuracy of the spacer pressure loss obtained by this method is estimated to be within $\pm$ 40%.

The triangular cell method of obtaining fuel rod spacer pressure loss requires that the spacer region be divided into flow cells, as exhibited in Figure 4, and that a pressure loss equation be written for one of these cells (p. 11). Disregarding fuel rod support fingers, each fuel rod is surrounded by six cells with this cross section. Four cells, type (d), are 0.5 in. long, the other two, type (c), are 1.0 in. long. Pressure loss due to the spacers is determined by writing a loss equation for a type (c) cell and then multiplying it by the number of spacers. The friction factor segment of the equation is multiplied by 1.1 to account for additional pressure loss due to fuel rod support fingers.

Two problems arise in applying this equation. First is the determination of sodium velocity in a (c) cell, V_c. The second is in obtaining

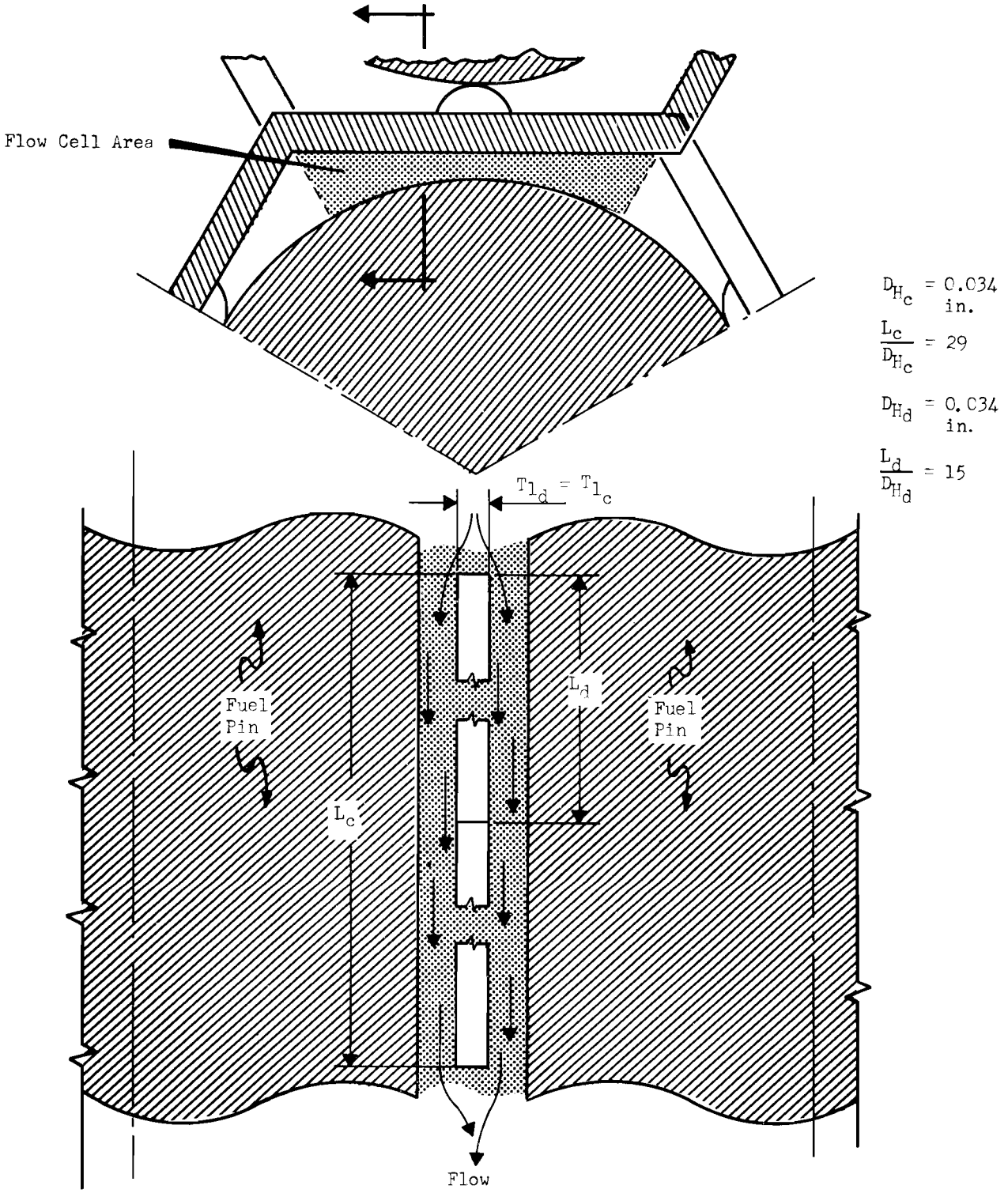

FIGURE 4. Type (c) or (d) Fuel Rod Spacer Flow Cell

the average Fanning friction factor, f_c, for a (c) cell. Because velocity is not known, the friction factor cannot be found. However, the average velocity of the sodium flowing through a spacer and the flow areas of the six cells surrounding a fuel rod are known. Therefore, an equation defining the flow rate through the six cells and one equating pressure loss through a (c) cell to that through a (d) cell can be solved simultaneously to obtain the required friction factor and velocity.

Average Fanning friction factors f_c and f_d are:

$$f_c = \frac{n_6 f_c^+ L_{11}}{W_c} + \frac{f_c^{++} \pi D_r}{6 W_c}$$

$$f_d = \frac{f_d^+ L_{11}}{W_d} + \frac{f_d^{++} \pi D_r}{6 W_d}$$

Approximate values of f_c^+ and f_d^+, which apply for cell walls formed of spacer strips, can be obtained for Reynolds numbers up to 1×10^4 from Reference 5, since they are assumed to equal the average factors for a stainless steel, type (t) cell as depicted in Figure 5.

Pressure loss due to the misalignment of spacer strips forming one wall of a (c) cell is accounted for by multiplying f_c^+ by 1.2. The value 1.2 is used because Reference 5 indicates that a percentage increase in friction factor due to burrs and edge curling is approximately 20%. It is assumed that this increase will account for the edge that projects into the flow stream due to spacer strip misalignment.

Although the parameters and geometry of a (t) cell are as close to a (c) or (d) cell as is given in Reference 5, comparison of Figures 4 and 5 indicates that differences exist. The effect of these differences

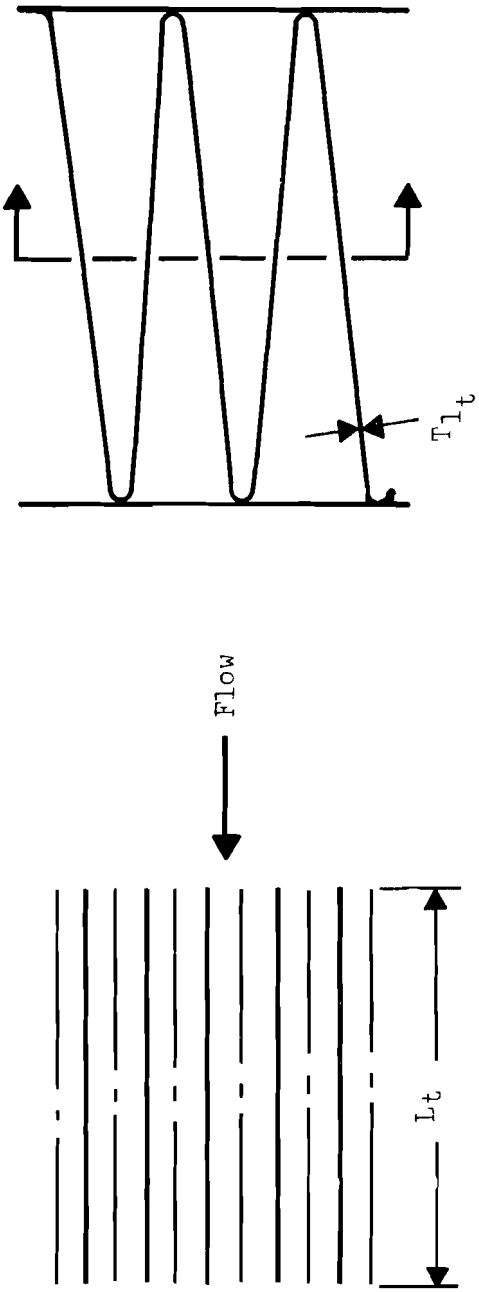

$D_{H_t} = 0.113$ in.

$\frac{L_t}{D_{H_t}} = 22$

FIGURE 5. Type (t) Triangular Flow Cell

on the validity of assuming similarity between friction factors for (c) or (d) cell walls formed of fuel rod spacer strips and average factors for a (t) cell (Reference 5) can only be roughly approximated. For the Reynolds numbers in question ($R \geq 2.0 \times 10^4$) friction factors for various cell geometries, hydraulic diameters, wall thicknesses, and length to hydraulic diameter ratios approach a value of 0.007 with maximum deviations of $\pm$ 15%.

Average Fanning friction factors f_c^{++} and f_d^{++} are assumed to equal those for smooth pipe. They apply for flow cell walls formed of fuel rods.

$$f_c^{++} = \frac{0.184}{R_c^{0.2}} \quad \pm 4$$

$$f_d^{++} = \frac{0.184}{R_d^{0.2}} \quad \pm$$

As shown on page 14, average Fanning friction factors f_c and f_d are determined by multiplying plus (+) and double plus (++) factors by the length of wetted perimeter for which they apply, summing the products, and then dividing by the cell wetted perimeter. Factors f_c and f_d are estimated to be accurate within $\pm$ 20%.

Entrance and exit loss coefficients for the cells are not included in f_c or f_d, but they are added to the friction factor part of the cell pressure loss equation. Entrance and exit loss coefficients K_4 and K_5 are $0.22^{(5)}$ and $0.10^{(5)}$, respectively. These coefficients are obtained by using a σ_c equal to 0.70 and entrance and exit loss lines for a Reynolds number of infinity since the Reynolds number is relatively high.

Final form of this fuel rod spacer pressure loss equation includes: entrance and exit losses for each spacer, loss due to fuel rod support fingers, and loss due to misalignment of spacer strips forming flow cell walls. It does not account for fluid mixing within spacers. Obtaining pressure loss due to the fuel rod spacers by this method is estimated to be accurate within $\pm$ 15%.

In the rectangular cell method, the fuel rod spacer region is divided into equivalent cells as illustrated in Figure 6, and a pressure loss equation is written for this type of cell (p. 11). The friction factor segment of this equation is multiplied by 1.1 to account for additional pressure loss due to fuel rod support fingers, and the whole equation is multiplied by the number of spacers.

Sodium velocity in an (o) cell, V_o, is assumed to equal the average velocity within a fuel rod spacer, V_s. There will also be some velocity variation within a cell, but it is assumed that any error introduced into the calculated pressure loss by this variation will average itself out.

Determining f_o, the average Fanning friction factor for an (o) cell, is the main problem in applying this equation.

$$f_o = \frac{n_7 f_o^{+}(W_o - \pi D_r) + f_o^{++}\pi D_r}{W_o}$$

Friction factor f_o^{+} applies for cell walls formed of spacer strips. It is assumed to equal the factor for an aluminum cell, type (s), as shown in Figure 7, which can be found for Reynolds numbers up to 1×10^4 in Reference 5. For higher Reynolds numbers, extrapolation

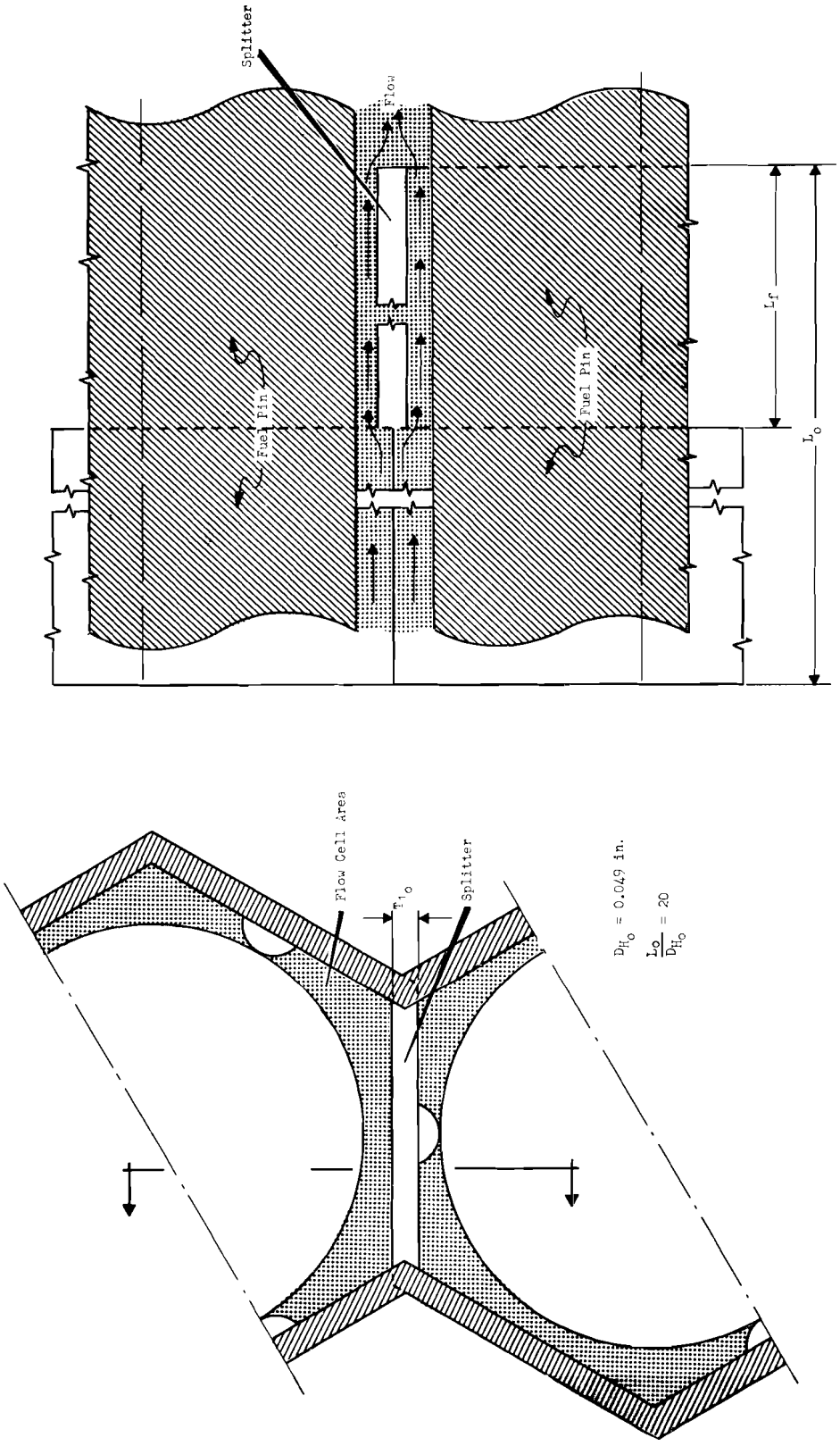

FIGURE 6. Type (o) Fuel Rod Spacer Flow Cell

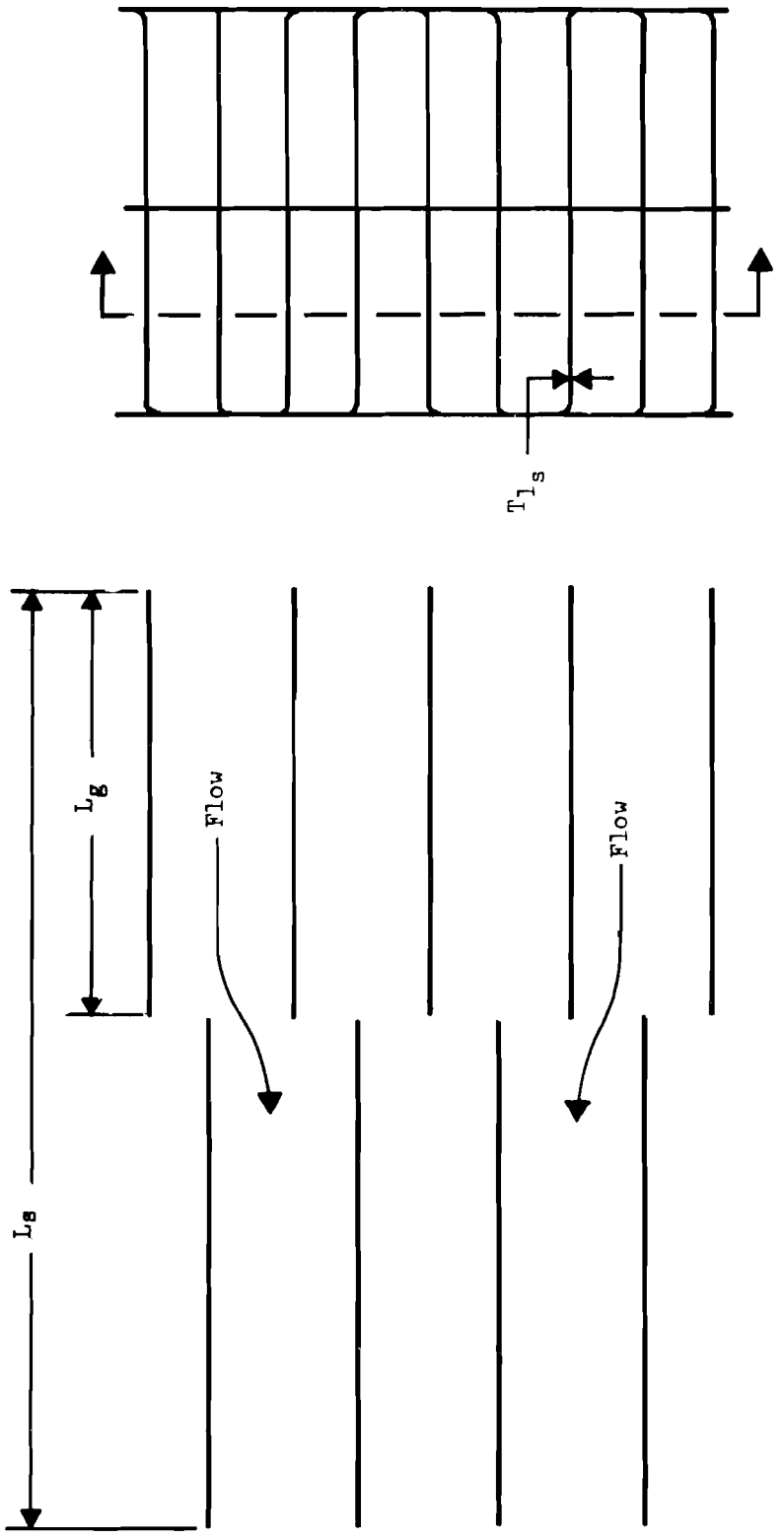

$D_{H_s} = 0.089$ in.

$\frac{L_s}{D_{H_s}} = 11$

FIGURE 7. Type (s) Rectangular Flow Cell

is necessary. The factor obtained from Reference 5 includes a component that accounts for increased pressure loss due to misalignment of spacer strips forming flow cell walls. However, it must be multiplied by 1.2 as recommended in the reference since the cells in question are stainless steel and, consequently, have a friction factor that is approximately 20% higher than for an aluminum cell because of fabrication-created burrs and edge curling.

There are parametric and geometric differences between an (s) and (o) cell as can be seen by examining Figures 6 and 7. Because of these differences, several cells with splitters were considered with various hydraulic diameters, wall thicknesses, uninterrupted flow lengths, and length to hydraulic diameter ratios. It was discovered that length of uninterrupted flow is the parameter that has the most pronounced effect on average friction factors.

Variation of uninterrupted flow length from 1/2 in. to 1/8 in. can increase the friction factor by 100% while changing other parameters results in a maximum friction factor variance of $\pm$ 15%. Therefore, an average factor for an (s) cell is used for f_o^+ because it is the only cell included in Reference 5 with a splitter and the same length of uninterrupted flow as an (o) cell.

Average Fanning friction factor f_o^{++} is assumed to equal that for smooth pipe. It applies for cell walls formed of fuel rods.

$$f_o^{++} = \frac{0.184}{R_o 0.2}$$

As shown on page 17, f_o is determined by multiplying plus (+) and double plus (++) factors by the length of wetted perimeter for which they apply, summing the products, and then dividing by the cell wetted perimeter. Its accuracy is estimated to be within ± 20%.

Entrance and exit loss coefficients for an (o) cell are not included in f_o, but they are added to the friction factor segment of the cell pressure loss equation. Entrance and exit loss coefficients K_6 and K_7 are 0.22[5] and 0.10[5], respectively. These values are obtained by using $a\sigma_o$ equal to 0.70 and entrance and exit loss lines for a Reynolds number of infinity since the Reynolds number is relatively high.

This method of determining fuel rod spacer pressure loss includes: entrance and exit losses for each spacer, loss due to fuel rod support fingers, loss due to misalignment of spacer strips forming flow cell walls, and fluid mixing within spacers. Pressure loss due to the fuel rod spacers, as obtained by this method, is estimated to be accurate within ± 15%.

Pressure loss $\Delta p_{6'-7'}$ is due to skin friction in the fuel rod bundle between positions 6-6 and 7-7. A rod bundle flow cell is defined as shown in Figure 8. Pressure loss for flow through this cell is assumed to equal that of a round pipe having the same equivalent diameter, surface roughness, length, and fluid velocity. This approach is suggested in Reference 4, and is estimated to be accurate within ± 5%.

$$\Delta p_{6'-7'} = \frac{f_x L_x V_x^2 \rho}{D_{H_x} 2g}$$

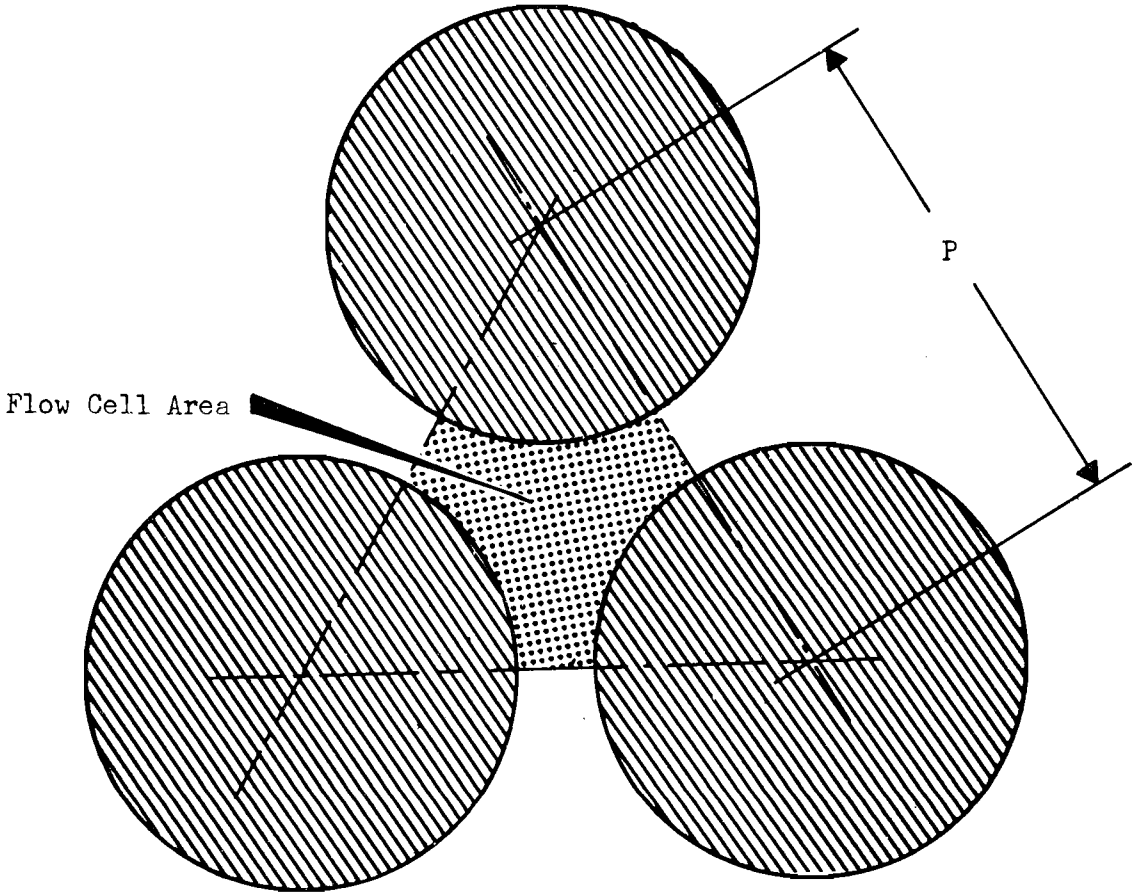

FIGURE 8. Fuel Rod Bundle Central Flow Cell

Average Moody friction factor f_x is:

$$f_x = \frac{0.184}{R_x 0.2}$$

Length L_x is equal to the active fuel rod length, L_5, minus the length of fuel rod within the fuel rod spacers.

Pressure loss Δp_7 is due to exit effects that occur as sodium leaves the fuel rod bundle at position 7-7.

$$\Delta p_7 = \frac{K_8 V_5^2 \rho}{2g}$$

For a σ_1 of 0.36 and an exit loss line for a Reynolds number of infinity since the Reynolds number is relatively high, loss coefficient K_8 is 0.42[5].

Pressure loss Δp_9 is due to exit effects that occur as sodium leaves the fuel element and enters the upper plenum.

$$\Delta p_9 = \frac{K_9 V_6^2 \rho}{2g}$$

Exit loss coefficient K_9 is 1.00[3] since all fluid kinetic energy is assumed to be dissipated in the plenum.

Pressure loss Δp_{1-9} is due to the change in static head between positions 1-1 and 9-9. Assuming that the process tubes are vertical, the defining equation is:

$$\Delta p_{1-9} = L_4 \gamma$$

Solution of the General Equation

Individual equations for each component of the fuel element pressure loss are combined into the general pressure loss equation. Then assumed and calculated values are inserted for all unknowns, and fuel

element pressure loss is calculated. The velocities necessary to solve the general equation are calculated knowing fuel element mass flow rate and flow areas. Sodium mass flow rate through each fuel rod bundle of a 300 MW_t reactor containing the equivalent of 53-1/2 driver fuel elements is 57 lb/sec. Sodium density and temperature rise through a fuel element were assumed to be 54.2 lb/ft and 300 ^{o}F, respectively. This mass flow rate includes a factor of safety since approximately 6% of the 300 MW_t is generated by neutron and gamma radiation outside the core. Mass flow rate through all driver fuel elements is assumed to be the same since power generation per fuel element is approximately the same due to zone fueling.

FUEL ELEMENT ANNULUS HYDRAULICS

Sodium flow in the spiral channel annulus existing between the fuel element liner and process tube is examined in this analysis. These channels extend from positions 6-6 to 8-8 as depicted in Figure 1. Position numbers mentioned in the text refer to lines on the fuel element as illustrated in this figure.

General Pressure Loss Equation

The general equation defining annulus pressure loss between positions 6-6 and 8-8 is:

$$\Delta p_{ann} = \Delta p_{6} + \Delta p_{6'} + \Delta p_{6-8} + \Delta p_{6'-8'} + \Delta p_{8} + \Delta p_{6''-8''}$$

Annulus pressure loss, as obtained by using this equation, is estimated to be accurate within $\pm$ 10%.

Pressure loss Δp_{6} is due to entrance effects that occur as sodium enters the spiral channels at position 6-6. The equation indicated below is estimated to produce results that are accurate within $\pm$ 10%.

$$\Delta p_{6} = \frac{K_5 V_5^{2} \rho}{2g}$$

Entrance loss coefficient K_5 is 0.70 [2]. This coefficient is for a sharp-edged entrance as exhibited in Figure 3.

Pressure loss $\Delta p_{6'}$ is due to sodium acceleration at position 6-6 from a path parallel to the fuel element to one inclined at a spiral angle (θ) as illustrated in Figure 9.

$$\Delta p_{6'} = \frac{(\cos \theta)^2 V_5^2 \rho}{2g}$$

Pressure loss Δp_{6-8} is due to skin friction in the channels between positions 6-6 and 8-8.

$$\Delta p_{6-8} = \frac{f_5 L_5 V_5^2 \rho}{D_{H_5} 2g}$$

Average Moody friction factor f_5 is:

$$f_5 = \frac{0.184}{R_5^{0.2}}$$

Results of this equation are estimated to be accurate within $\pm$ 5%.

Pressure loss $\Delta p_{6'-8'}$ is due to bends in the channels between positions 6-6 and 8-8.

$$\Delta p_{6'-8'} = \frac{n_1 K_6 V_5^2 \rho}{2g}$$

Calculations show that for the assumed bend dimensions, loss coefficient K_6 is 0.024 [1]; however, it will vary if the bend dimensions are changed. Results of this equation are estimated to be accurate within $\pm$ 5%.

Pressure loss Δp_8 is due to exit effects that occur as sodium leaves the spiral channels at position 8-8.

$$\Delta p_8 = \frac{K_7 V_5^2 \rho}{2g}$$

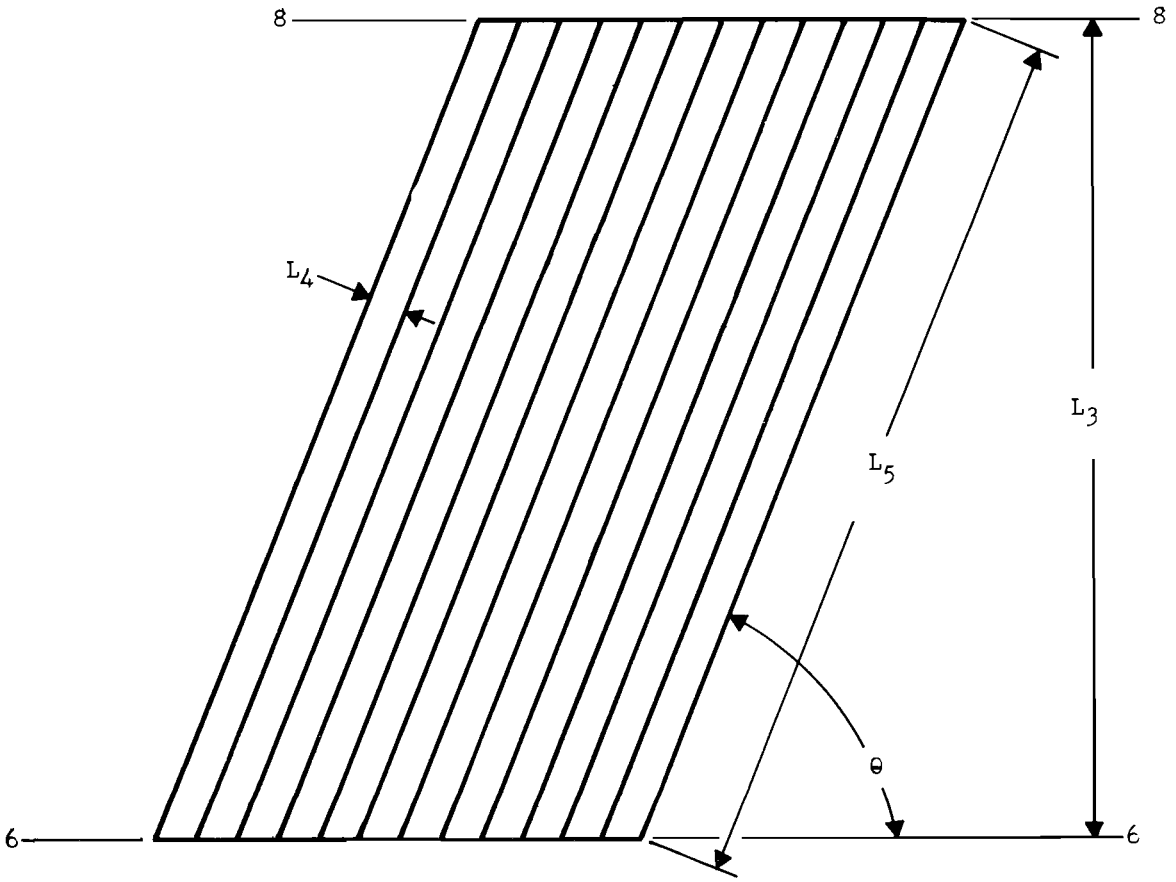

FIGURE 9. Plan View of Fuel Element Liner with Spiral Ribs Attached

Loss coefficient K_7 is 1.00[3] since a large share of the fluid kinetic energy will be dissipated in turbulence at this position.

Pressure loss $\Delta p_{6"-8"}$ is due to the change in static head between positions 6-6 and 8-8. Assuming that the process tubes are vertical, the defining equation is:

$$\Delta p_{6"-8"} = L_3 \gamma$$

Solution of the General Equation

Individual equations for each component of the annulus pressure loss are combined into the general pressure loss equation, and the assumed and calculated values are inserted for all unknowns except sodium velocity in the annulus, V_5, and annulus pressure loss, Δp_{ann}. Since annulus and fuel element pressure losses are equal between position 6-6 and 8-8, the annulus pressure loss equation is solved by inserting a sodium velocity that will produce an annulus pressure loss equal to a reasonable value of fuel element pressure loss between these positions (28 fps).

SODIUM LEAKAGE BETWEEN ANNULUS SPIRAL CHANNELS

Sodium leakage between annulus spiral channels that are sandwiched by the fuel element liner and process tube is being determined in this investigation. These channels extend from positions 6-6 to 8-8 as illustrated in Figure 1. Position numbers mentioned in the text refer to lines on the fuel element as depicted in this figure.

Equations

Assuming viscous flow, the equation for determining total sodium flow

rate between annulus spiral channels, M_c, is:

$$M_c = \frac{L_1^2 A_c n_2 \Delta p_c g \rho}{12 L_5 \mu} \quad (12)$$

The pressure differential across an annulus spiral rib, Δp_c is:

$$\Delta p_c = \frac{\Delta p_{ann}}{n_1 n_2}$$

This equation indicates that pressure difference across a rib is equal to annulus pressure loss between positions 6-6 and 8-8 divided by the number of flow channels crossed by a line parallel to the fuel element between these positions, which implies that pressure decreases in equal increments from channel center to center along this line and that pressure difference between adjacent channel centers is the pressure differential across a rib. This is not exactly true, but it is the worst foreseeable condition. Therefore, if cross channel leakage is low for this case, the actual case will be of no concern.

Solution of Sodium Leakage Equation

Pressure differential, Δp_c, is calculated, and it is inserted into the sodium leakage equation along with assumed and calculated values for other unknowns. Solving this equation results in total sodium leakage between annulus spiral channels.

FUEL ROD SPACER STRENGTH

In this study, strips forming the fuel rod spacers (spacer strips) are examined by two methods to determine if they can withstand the fluid forces exerted on them. Fuel rod spacer geometry is exhibited in Figure 2.

Shear Analysis

(1) Equations. This method assumes that a spacer strip is supported

only where it is attached to the fuel element liner. Shear stress in the strip is determined by:

$$\sigma_g = \frac{F_1}{A_1}$$

Force F_1 is the total drag force on the longest strip.

$$F_1 = \frac{C_D A_2 V_5^2 \rho}{2g}$$

Coefficient of drag for a spacer strip, C_D, is 2.00[3]. This coefficient is for a square bar with fluid flowing transverse to its longitudinal axis, which is the worst foreseeable condition. Estimated accuracy of σ_g, F_1, and C_D is within ± 50%.

(2) Solution. The actual force on a spacer strip, F_1, is calculated, and this value is divided by the shear area, A_1, to obtain the shear stress in a spacer strip, σ_g. Stress, σ_g, is then divided into the minimum yield stress to obtain the safety factor.

Column Analysis

(1) Equations. In this approach a section of spacer strip with length L_{11}, as shown in Figure 10, is studied. It is assumed that this section is not supported by any other member and that it might fail by column action due to the force acting on it, F_2.

$$F_2 = \frac{F_1 L_{11}}{L_{14}} = \frac{F_1}{2n_4}$$

The force, F_2, is assumed to act at the section ends as exhibited in Figure 10 and is estimated to be accurate within ± 50%. Making this assumption assures that the worst force condition is considered.

Euler's equation is used to determine P_{cr}, the maximum allowable section load, since r^2 divided into Q is 5.3.

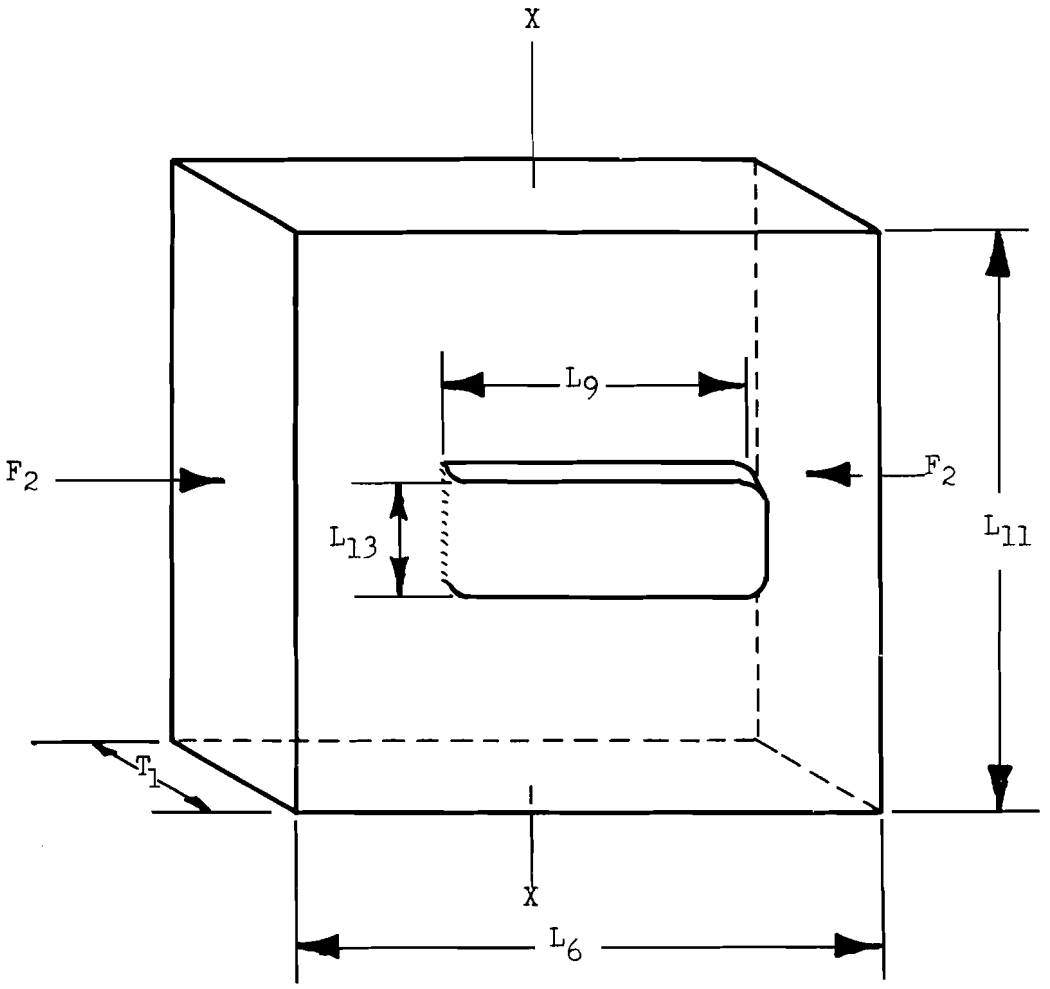

FIGURE 10. Section of Fuel Rod Spacer Strip

$$P_{cr} = \frac{S_y A_3 r^2}{Q} \quad (8)$$

Defining equations for the least radius of gyration, r, and for the factor Q are:

$$r = (0.289)\ T_1$$

$$Q = \frac{S_y L_6^2}{n_2 \pi^2 E}$$

As stated previously, yield stress is 18,500 psi and the modulus of elasticity is 19.2×10^6 psi[13] for 304 stainless steel at a temperature of 1000°F. The coefficient accounting for section end conditions, n_2, is 0.25[8].

(2) Solution. The force on each section of spacer strip, F_2, and the maximum allowable section load, P_{cr}, are calculated. Then the latter is divided by the former to obtain the factor of safety.

EVALUATION

FUEL ROD BUNDLE HYDRAULICS

Fuel element pressure loss as found by the de Stordeur, triangular cell, and rectangular cell methods i s 99 ± 30%, 125 ± 15%, and 129 psi ± 15%, respectively. Pressure losses given by the de Stordeur and triangular cell methods are 77 and 97%, respectively, as large as that given by the rectangular cell method. This is a range of 23%.

Figure 11 shows each component of fuel element pressure loss as a percentage of the fuel element loss given by the rectangular cell method. As can be seen, the fuel rod spacer component is largest; it is equal to 80 psi ± 15% and accounts for 62% of the fuel element loss. Other important components are anchor and spacer bar and skin friction losses which are responsible for 10 and 21% of fuel element loss, respectively.

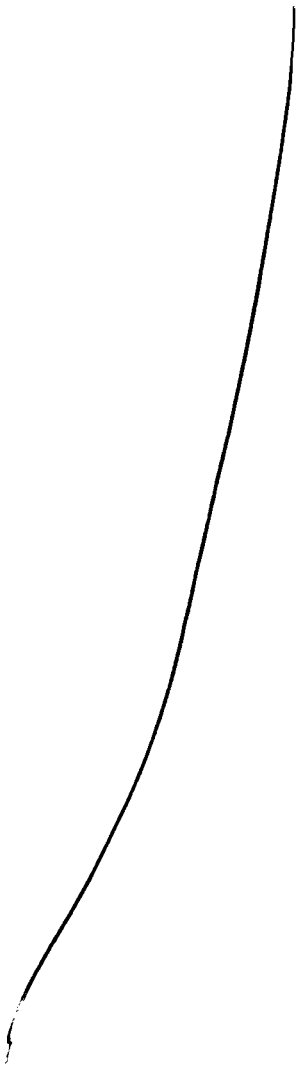

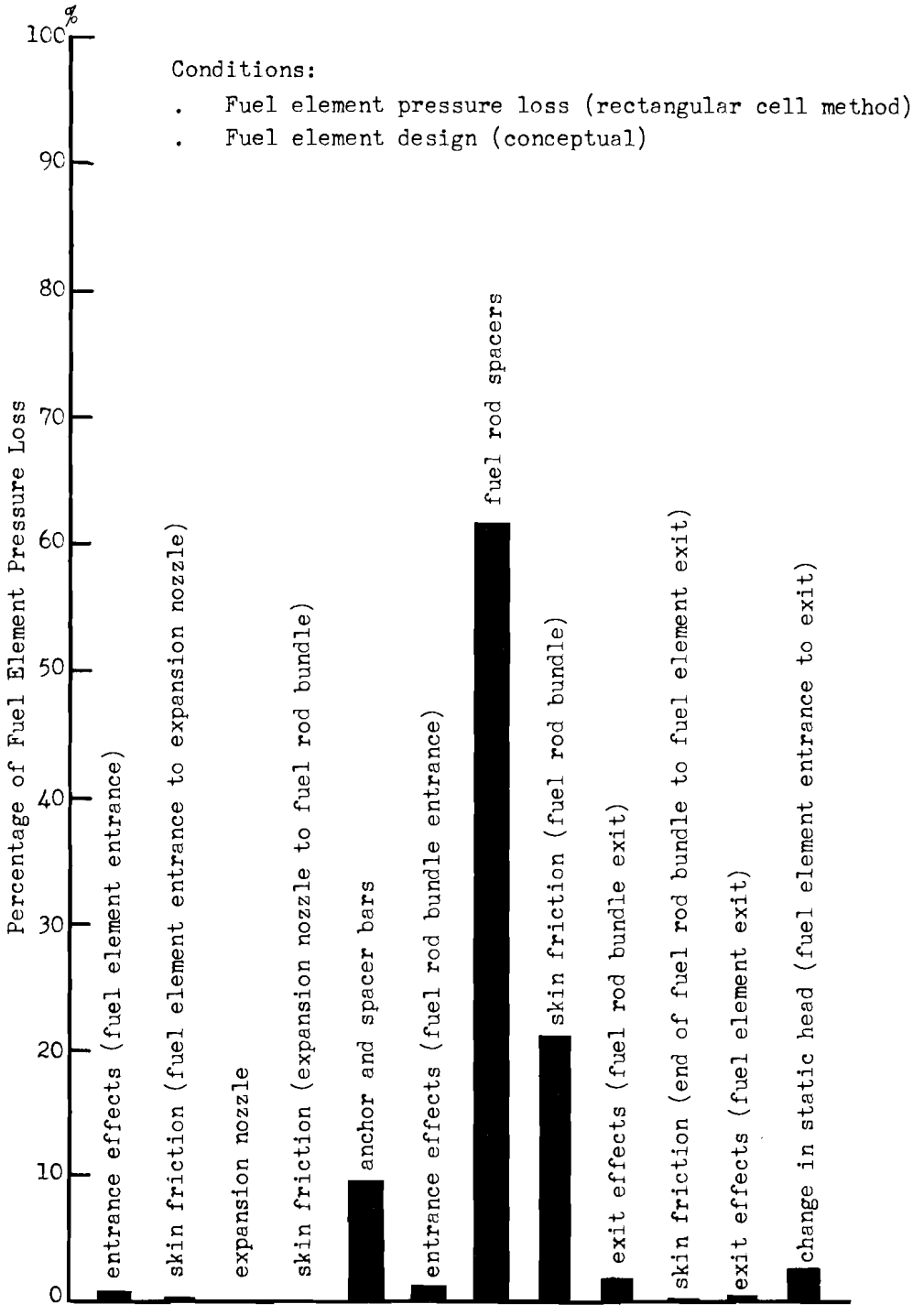

FIGURE 11. Driver Fuel Element Pressure Loss Components

Since the largest fuel element pressure loss component is due to fuel rod spacers, it is of interest to compare the percentage value of this component as given by each approach. For the de Stordeur, triangular cell, and rectangular cell methods, fuel rod spacer loss amounts to 54 $\pm$ 40%, 77 $\pm$ 15%, and 80 psi $\pm$ 15%, respectively. Percentage of fuel element pressure loss associated with the value produced by each method is, in the order stated previously, 54, 61, and 62%. This is a range of 8% which indicates that even through fuel element pressure loss as given by each method may vary by as much as 23%, fuel rod spacer loss as a percentage of fuel element loss remains fairly stable.

It should be noted that in order to simplify solution of the general pressure loss equation, volumetric flow rate through the fuel rod bundle is assumed to equal the total flow rate through the fuel element at position 2-2. It is also assumed that holes are drilled through the fuel element liner at position 4-4 as well as 6-6. The first assumption introduces a small error into the calculated fuel element pressure loss since some flow is diverted through the annulus. For a given rod bundle flow rate, velocities V_1, V_2, and V_6 are higher than assumed in this analysis. Actual values of these velocities can be found by multiplying them by the ratio of fuel element to fuel rod bundle volumetric flow rate, Q_t/Q_4. However, pressure loss components involved are so small that error introduced into the calculated fuel element pressure loss is less than 1%.

Main contributors to fuel element pressure loss, as mentioned previously, are the fuel rod spacers, anchor and spacer bars, and fuel rod bundle skin friction. Ways of reducing these losses need to be examined because fuel element loss, as given by all three pressure loss methods is above a maximum design value of 80 psi for the required fuel rod bundle mass flow rate of 57 lb/sec by 49 psi $\pm$ 40% (rectangular cell method).

Three ways of reducing fuel rod spacer pressure loss are to remove one or more sets of spacers (one set), to use elastic support dimples instead of support fingers, and to decrease spacer strip thickness (0.015 to 0.010 in.). Reduction of fuel element pressure loss by each modification is 10, 4, and 24%, respectively. Other ways of reducing this loss, that were not included in this study but will be considered later, are to reduce spacer strip width; to use spacer strips with a lenticular cross section; and to decrease the number of fuel rods or their diameter.

Pressure losses due to the anchor and spacer bars and fuel rod skin friction can also be reduced. Two ways of decreasing anchor and spacer bar pressure loss are to use bars with a lenticular cross section and to reduce the bar thickness. Reducing the number of fuel rods, their diameter, or length, are the only ways to decrease pressure loss due to fuel rod bundle skin friction. Reduction of fuel element pressure loss by any of these modifications is not covered in this report, but they are mentioned here to draw attention to the possibilities.

It should be noted that because of fuel rod spacer geometry, some spacer flow areas will be restricted more than others. The resulting flow rate variation throughout the spacer flow area not only will cause a pressure

loss due to fluid mixing but will also hinder even fuel rod cooling. Some flow areas, those that exist between a fuel rod and section of fuel rod spacer where top and bottom spacer strips align, will be starved of flow to the point that hot spots will probably occur on the fuel rod. Fluid mixing will promote, somewhat, even fuel element cooling, but whether the advantage of mixing outweighs the disadvantages of increased pressure loss, and uneven fuel rod cooling needs to be examined in more detail. One solution is to redesign the fuel rod spacers. It should also be noted that if support fingers as depicted in Figure 2 are used, the free ends should be downstream so that fuel element pressure loss will not be increased by additional fluid mixing.

The results of this study are required for further parametric studies which are necessary to achieve an optimum fuel design.

FUEL ELEMENT ANNULUS HYDRAULICS

Inserting a sodium velocity of 28.0 fps in the annulus pressure loss equation results in an annulus pressure loss of 70.0 psi $\pm$ 10%. If an average sodium density of 54.2 lb/ft^3 is used in calculating mass flow rate, it is 6.7 lb/sec.

Annulus pressure loss components are exhibited as percentages of annulus pressure loss in Figure 12. It can be seen from this figure that the major component is due to channel skin friction, which accounts for 84% of the pressure loss. In psi form, it is equal to 59 psi $\pm$ 5%. The only other losses large enough to mention are due to channel entrance and exit effects which account for 5 and 7% of the pressure loss, respectively.

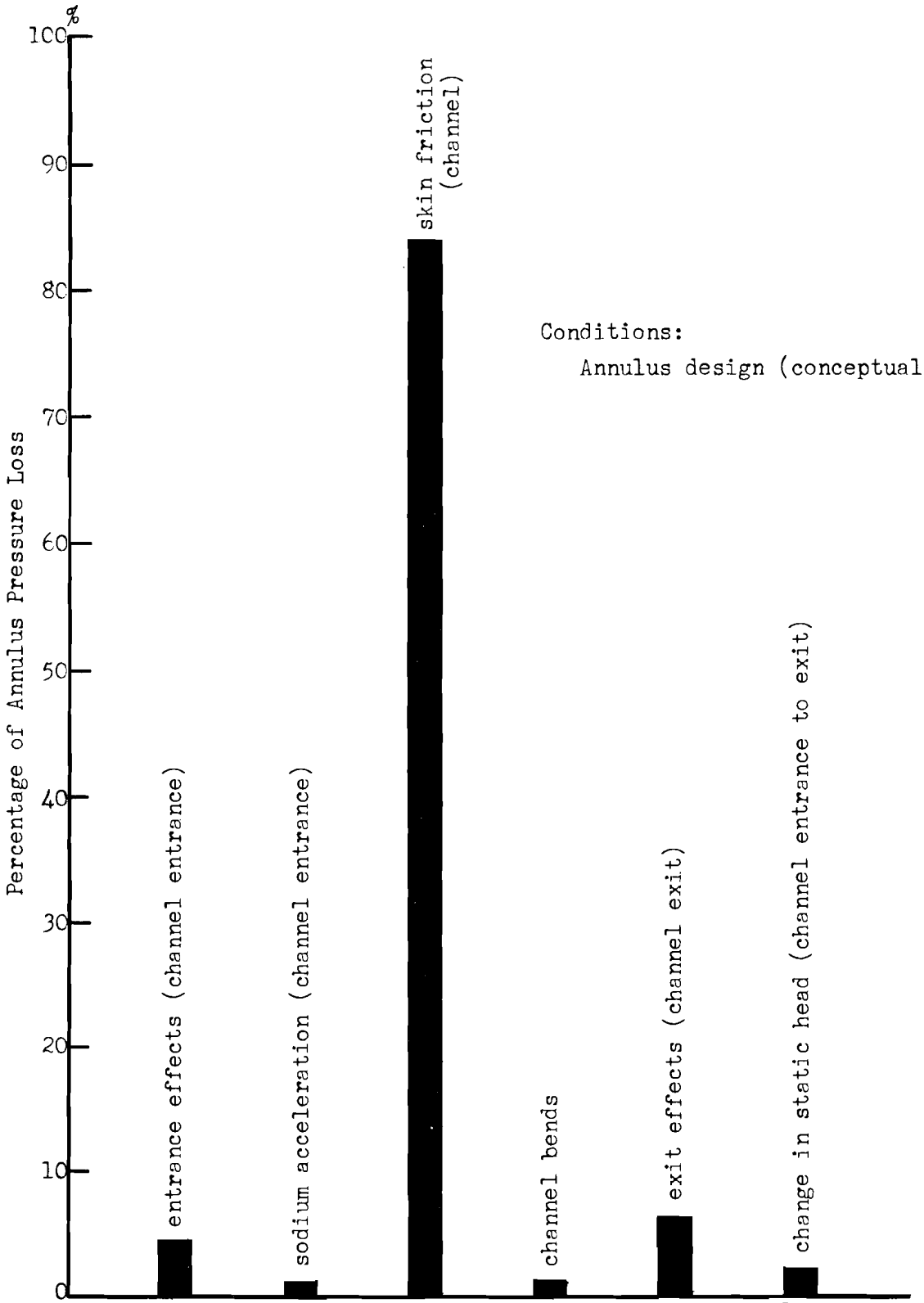

FIGURE 12. Driver Fuel Element Annulus Pressure Loss Components

Since fuel rod bundle and annulus pressure losses do not take place in the same manner, a pressure difference exists across the fuel element liner. For a fuel element sodium flow rate of 57 lb/sec and corresponding rod bundle and annulus pressure losses (rod bundle pressure loss obtained by the rectangular cell method), this differential is 36 psi maximum as indicated in Figure 13. It can be reduced to 7 psi and annulus sodium flow rate increased by drilling holes in the fuel element liner at position 7-7. The dashed line shown in Figure 13 represents annulus pressure loss as a function of fuel element length after drilling the holes. Pressure difference across the fuel element liner is measured away from a fuel rod spacer since there is a grid band between fuel rod bundle and annulus sodium flow at spacer positions.

Variation and interaction of annulus pressure loss, Δp_{ann}, channel spiral angle (θ), channel hydraulic diameter, D_{H_5}, and sodium velocity in the annulus, V_5, is important because of the need for predicting a combination of annulus hydraulic parameters that will promote uniform fuel element cooling* most effectively. A parameter study was carried out by computer and hand calculations for an annulus length, L_3, of 4.3 ft using the equation:

$$\Delta p_{ann} = \frac{V_5^2 \rho}{2g\,144}\left[1.70 + (\cos\theta)^2 + \frac{1.3}{(V_5)^{0.2}(D_{H_5})^{1.2}\sin\theta} + \frac{(21.74)K_6}{\tan\theta}\right] + 1.61$$

Bend loss coefficient K_6 in the preceding equation will vary with the parameters, but for calculations involving this equation, bend geometry is such that this coefficient can be assumed to remain constant at 0.024[1]. Estimated accuracy of Δp_{ann} or V_5 obtained by using this equation is within $\pm$ 10 and $\pm$ 6%, respectively.

* reduce radial fuel element temperature gradients

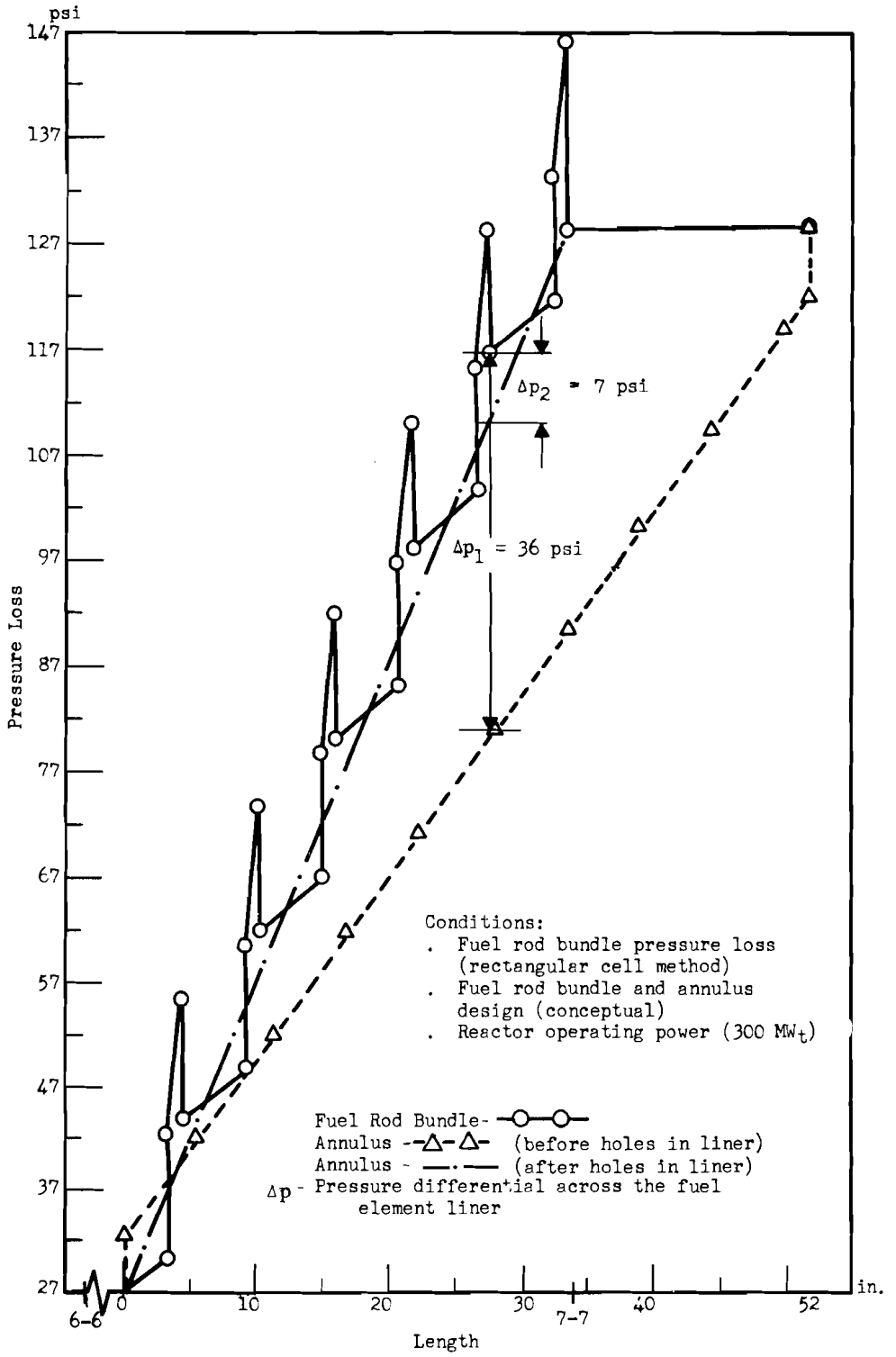

FIGURE 13. Driver Fuel Rod Bundle and Annulus Pressure Losses as a Function of Length

Figure 14 exhibits annulus pressure loss for a constant channel hydraulic diameter of 0.091 in.; sodium velocities in the annulus of 20, 25, and 30 fps; and spiral angles of from 50 to 75 degrees. As indicated, decrease in annulus pressure loss with increasing spiral angle is more pronounced at higher velocities and smaller spiral angles.

Annulus pressure loss for a constant channel spiral angle of 67 degrees; sodium velocities in the annulus of 15, 20, 25, and 30 fps; and channel hydraulic diameters of from 0.050 to 0.150 in. is indicated in Figure 15. As shown, decrease in annulus pressure loss with increasing values of hydraulic diameter is much more pronounced at higher velocities and smaller hydraulic diameters.

Figure 16 depicts sodium volumetric flow rate through the annulus for annulus pressure losses of 50.0, 60.0, and 70.0 psi; spiral angles of from 5 to 90 degrees; and a channel hydraulic diameter of 0.091 in. As can be seen, volumetric flow rate increases rapidly with an increase in spiral angle at small angles, but this method of varying flow rate becomes less effective as the angle is enlarged.

The parameter that appears to have the greatest effect on sodium flow in the annulus is the spiral channel hydraulic diameter. It should be noted that increasing channel height, T_5, by 300% enlarged the channel hydraulic diameter by 192%, but increasing channel width, L_4, by 275%, enlarges the hydraulic diameter by only 7%.

SODIUM LEAKAGE BETWEEN ANNULUS SPIRAL CHANNELS

Assuming a clearance between channels, L_1, 0.001 in., (maximum deviation + 100%) along the fuel channel length, L_5, and an annulus

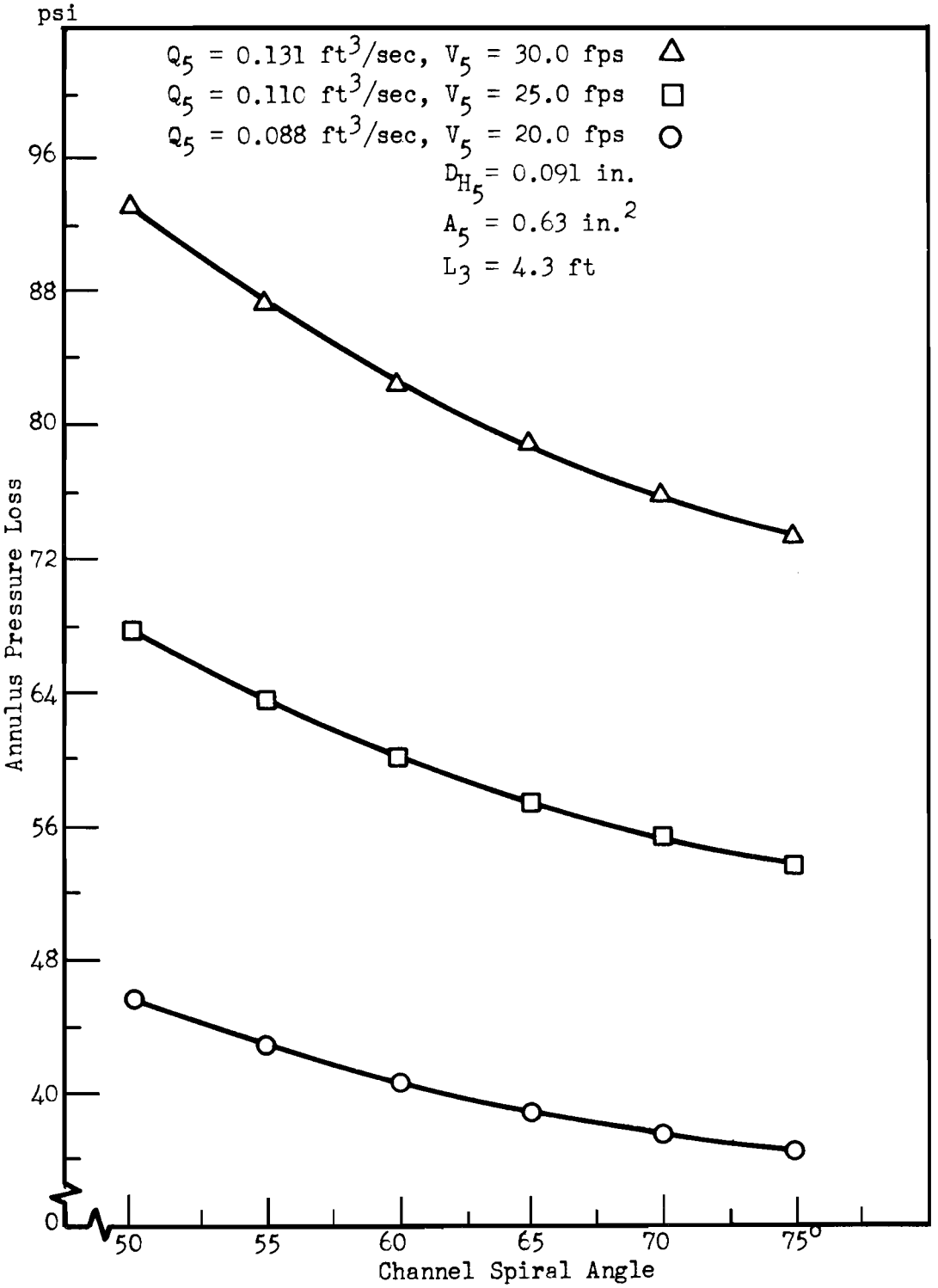

FIGURE 14. Annulus Pressure Loss for Various Channel Spiral Angles and Velocities

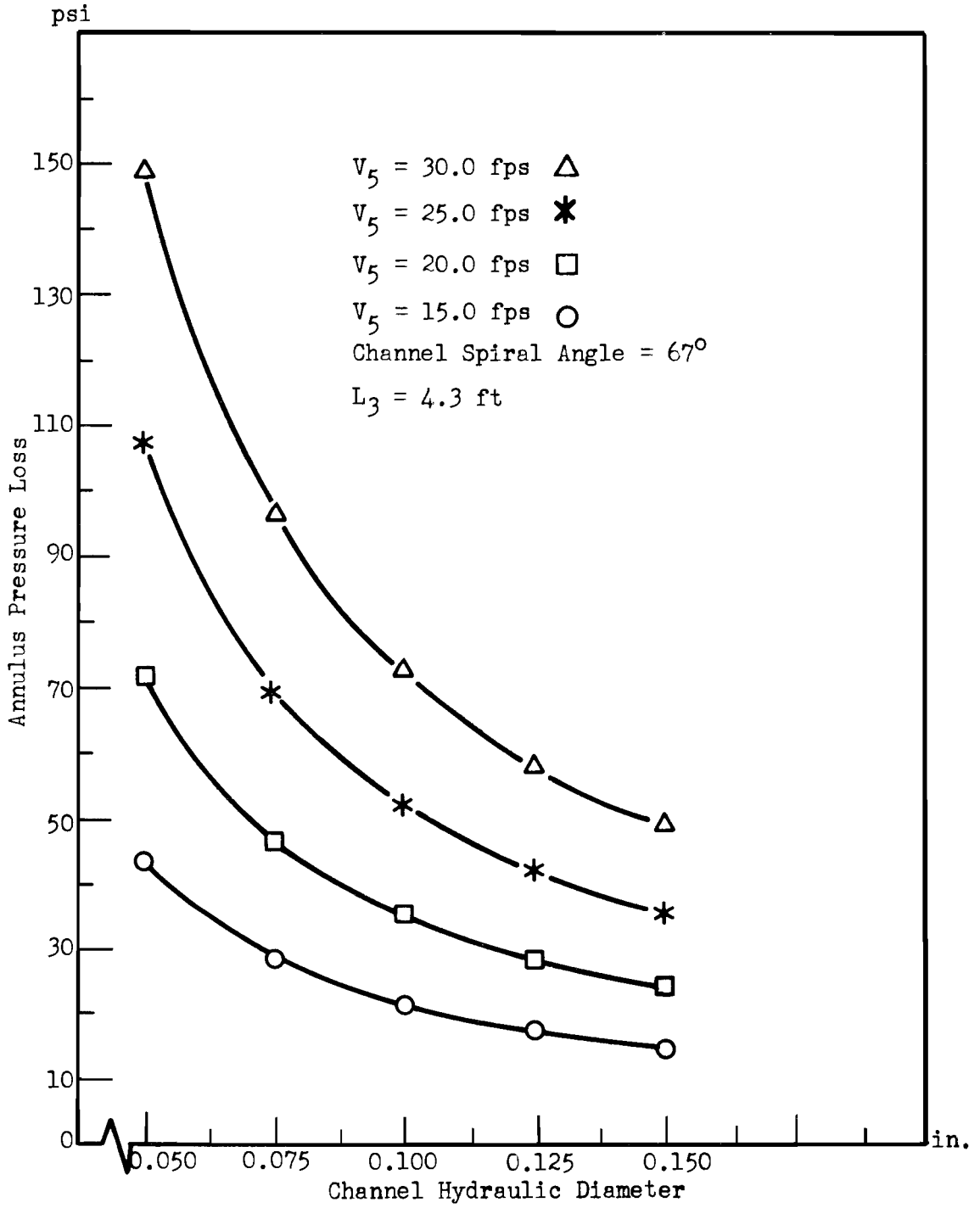

FIGURE 15. Annulus Pressure Loss for Various Channel Hydraulic Diameters and Velocities

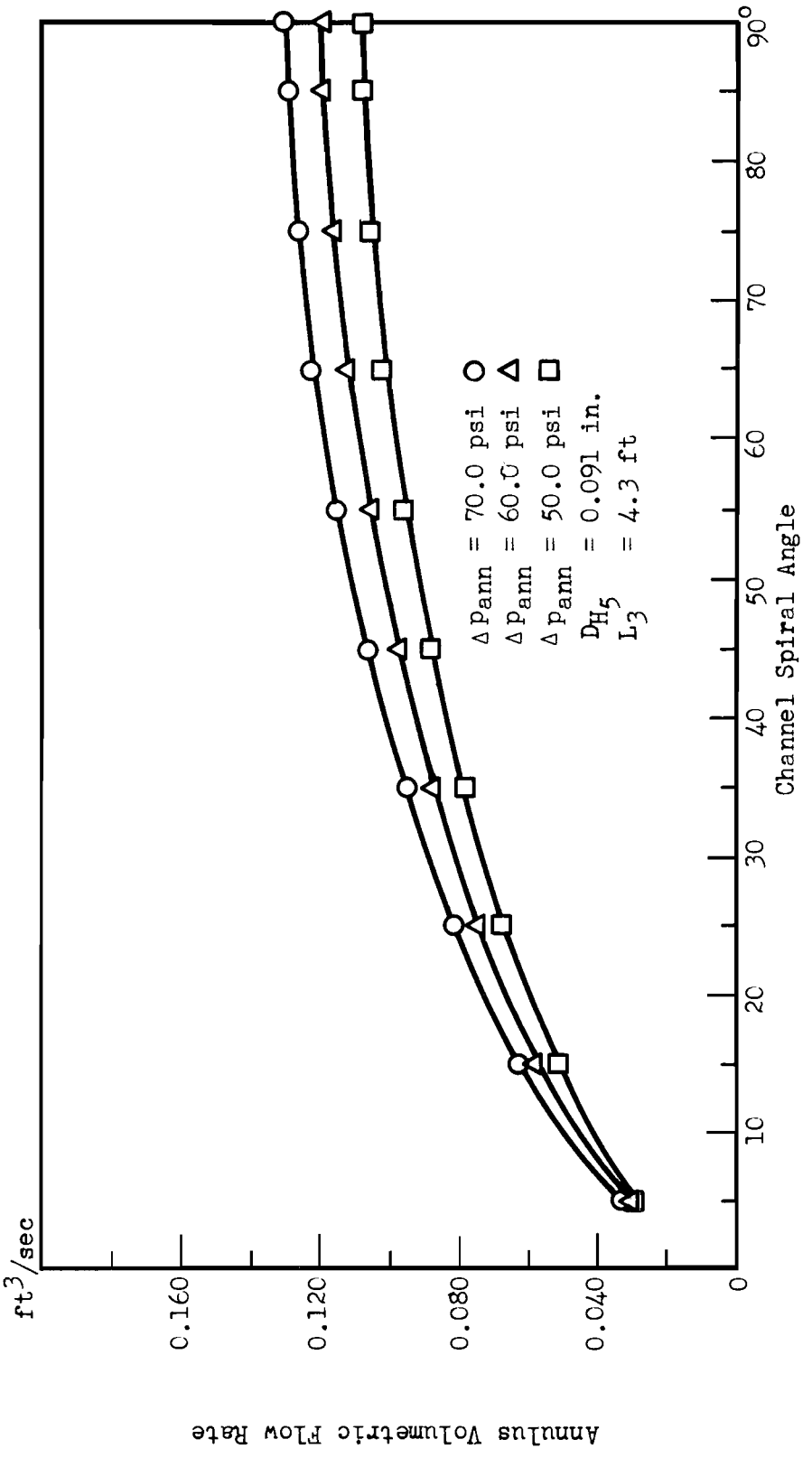
Annulus Volumetric Flow Rate
ft³/sec
0.160
0.120
0.080
0.040
0
10
20
30
40
50
60
70
80
90°
Channel Spiral Angle
Δ p_ann = 70.0 psi
Δ p_ann = 60.0 psi
Δ p_ann = 50.0 psi
D_H5 = 0.091 in.
L_3 = 4.3 ft

pressure loss, Δp_{ann}, of 70 psi, sodium mass flow rate between channels is 2.6×10^{-3} lb/sec + 700% which amounts to 3.9×10^{-2}% of sodium flow in the annulus. This indicates that leakage will decrease very little the spiral motion of sodium flow in the annulus that is necessary to promote uniform fuel element cooling even for the extreme of the values stated above.

FUEL ROD SPACER STRENGTH

Shear Analysis

Dividing the calculated value of force on a spacer strip (F_1 = 2.6 lb ± 50%) by the shear area of a strip (A_1 = 0.008 in^2) results in a spacer strip shear stress of 325 psi ± 50%. Based on a minimum yield stress of 18,500 psi[16] the factor of safety is 57. This yield stress was found by the 0.2% offset method for a metal temperature of 1000°F.

Column Analysis

The maximum allowable section load (P_{cr} = 6.3 lb) divided by the actual load (F_2 = 0.08 lb ± 50%) results in a safety factor of 79. For conditions as stated above and a 0.010 in. thick spacer strip, a column analysis predicts a minimum safety factor of 35.

These factors of safety indicate that spacer strip thickness can be reduced below 0.010 in. and still withstand the fluid forces. However, other considerations such as required fuel rod support finger force, cyclic loading of support fingers due to vibration, deterioration of metal properties due to irradiation, etc. will probably limit the reduction of spacer strip thickness. If further reduction is necessary, the possibility of using elastic support dimples instead of fingers should be investigated.

ACKNOWLEDGEMENTS

The author is grateful to R. J. Hennig, C. E. Leach, R. E. Peterson and D. S. Trent for their technical assistance.

NOMENCLATURE

FUEL ROD BUNDLE HYDRAULICS

All position numbers refer to lines on the fuel element as illustrated in Figure 1.

Lengths

(1) L_1 = Length of fuel element between positions 1-1 and 2-2 (ft)

(2) L_2 = Length of fuel element between positions 3-3 and 4-4 (ft)

(3) L_3 = Length of fuel element between positions 7-7 and 9-9 (ft)

(4) L_4 = Length of fuel element between positions 1-1 and 9-9 (ft)

(5) L_5 = Length of fuel element between positions 6-6 and 7-7 (ft)

(6) L_6 = Width of strips forming a fuel rod spacer (Figure 2) (in)

(7) L_7 = $2L_6$ Defined in Figure 2 (in)

(8) L_{10} = Defined in Figure 2 (in)

(9) L_{11} = Defined in Figure 2 (in)

(10) L_{12} = Height of a fuel rod support finger (Figure 2) (in)

(11) L_{13} = Width of a fuel rod support finger (Figure 2) (in)

(12) L_x = $L_5 - n_2 L_7$ (ft)

(13) L_c = Length of a type (a) or (c) fuel rod spacer flow cell (Figure 2) (in)

(14) L_d = Length of a type (d) fuel rod spacer flow cell (Figure 2) (in)

(15) L_o = Length of a type (o) fuel rod spacer flow cell (Figure 2) (in)

(16) L_s = Length of a type (s) flow cell (in)

(17) L_t = Length of a type (t) flow cell (in)

(18) L_f = Uninterrupted flow length of a type (o) fuel rod spacer flow cell (in)

(19) L_g = Uninterrupted flow length of a type (s) flow cell (in)

(20) T_1 = Thickness of the strips forming a fuel rod spacer or grid band (Figure 2) (in)

(21) T_{1_c} = Thickness of material forming walls of a type (c) fuel rod spacer flow cell (in)

(22) T_{1_d} = Thickness of material forming walls of a type (d) fuel rod spacer flow cell (in)

(23) T_{1_o} = Thickness of material forming walls of a type (o) fuel rod spacer flow cell (in)

(24) T_{1_s} = Thickness of material forming walls of a type (s) flow cell (in)

(25) T_{1_t} = Thickness of material forming walls of a type (t) flow cell (in)

(26) T_2 = Thickness of a spacer or anchor bar (Figure 2) (in)

(27) T_4 = Defined in Figure 2 (in)

(28) P = Triangular pitch of the fuel rods (Figure 2) (in)

Diameter

(1) D_r = Diameter of a fuel rod or guide pin (Figure 2) (in)

Wetted Perimeters

(1) W_c = Wetted perimeter of a type (c) fuel rod spacer flow cell (in)

(2) W_d = Wetted perimeter of a type (d) fuel rod spacer flow cell (in)

(3) W_o = Wetted perimeter of a type (o) fuel rod spacer flow cell (in)

Areas

(1) A_2 = Total flow area in the fuel element between positions 3-3 and 4-4 (in^2)

(2) A_5 = Total flow area in the fuel rod bundle between positions 6-6 and 7-7. This is away from a fuel rod spacer. (in^2)

(3) A_{p_s} = Projected frontal area of a fuel rod spacer. This includes fuel rod support fingers and a grid band. (in^2)

Hydraulic Diameters

(1) D_{H_1} = Hydraulic diameter of the fuel element between positions 1-1 and 2-2 (in)

(2) D_{H_2} = Hydraulic diameter of the fuel element between positions 3-3 and 4-4 (in)

(3) D_{H_3} = Hydraulic diameter of the fuel element between positions 7-7 and 9-9 (in) $D_{H_3} = D_{H_2}$

(4) D_{H_x} = Hydraulic diameter of a central fuel rod bundle flow cell. This is away from a fuel rod spacer. (in)

(5) D_{H_c} = Hydraulic diameter of a type (c) fuel rod spacer flow cell (in)

(6) D_{H_d} = Hydraulic diameter of a type (d) fuel rod spacer flow cell (in)

(7) D_{H_o} = Hydraulic diameter of a type (o) fuel rod spacer flow cell (in)

(8) D_{H_s} = Hydraulic diameter of a type (s) flow cell (in)

(9) D_{H_t} = Hydraulic diameter of a type (t) flow cell (in)

Velocities

(1) V_1 = Average sodium velocity in the fuel element between positions 1-1 and 2-2 (fps)

(2) V_2 = Average sodium velocity in the fuel element between positions 3-3 and 4-4 (fps)

(3) V_5 = Average sodium velocity in the fuel rod bundle between positions 6-6 and 7-7. This is away from a fuel rod spacer. (fps)

(4) V_6 = Average sodium velocity in the fuel element between positions 7-7 and 9-9 (fps)

(5) V_s = Average sodium velocity within a fuel rod spacer (fps)

(6) V_x = Average sodium velocity within a central fuel rod bundle flow cell. This is away from a fuel rod spacer. (fps)

(7) V_c = Average sodium velocity within a type (c) fuel rod spacer flow cell (fps) $V_c = V_s$

(8) V_o = Average sodium velocity within a type (o) fuel rod spacer flow cell (fps) $V_o = V_s$

Volumetric Flow Rates

(1) Q_t = Volumetric flow rate of sodium through the fuel element (ft^3/sec)

(2) Q_4 = Volumetric flow rate of sodium through the fuel rod bundle (ft^3/sec)

Friction Factors and Drag Coefficients

(1) f_1 = Average Moody friction factor for the fuel element between positions 1-1 and 2-2

(2) f_2 = Average Moody friction factor for the fuel element between positions 3-3 and 4-4

(3) f_3 = Average Moody friction factor for the fuel element between positions 7-7 and 9-9 $f_2 = f_3$

(4) f_x = Average Moody friction factor for a central fuel rod bundle flow cell. This is away from a fuel rod spacer.

(5) f_c = Average Fanning friction factor for a type (c) fuel rod spacer flow cell

(6) f_c^+ = Average Fanning friction factor for type (c) fuel rod spacer flow cell walls formed of spacer strips

(7) f_c^{++} = Average Fanning friction factor for type (c) fuel rod spacer flow cell walls formed of fuel rods

(8) f_d = Average Fanning friction factor for a type (d) fuel rod spacer flow cell

(9) f_d^+ = Average Fanning friction factor for type (d) fuel rod spacer flow cell walls formed of spacer strips

(10) f_d^{++} = Average Fanning friction factor for type (d) fuel rod spacer flow cell walls formed of fuel rods

(11) f_o = Average Fanning friction factor for a type (o) fuel rod spacer flow cell

(12) f_o^+ = Average Fanning friction factor for type (o) fuel rod spacer flow cell walls formed of spacer strips

(13) f_o^{++} = Average Fanning friction factor for type (o) fuel rod spacer flow cell walls formed of fuel rods

(14) C_s = Drag coefficient for a fuel rod spacer

Loss Coefficients

(1) K_1 = Entrance loss coefficient for the fuel element at position 1-1

(2) K_2 = Nozzle loss coefficient for the fluid expansion between positions 2-2 and 3-3

(3) K_3 = Entrance loss coefficient for the fuel rod bundle, positions 4-4 to 6-6

(4) K_4 = Entrance loss coefficient for a type (c) or (d) fuel rod spacer flow cell

(5) K_5 = Exit loss coefficient for a type (c) or (d) fuel rod spacer flow cell

(6) K_6 = Entrance loss coefficient for a type (o) fuel rod spacer flow cell

(7) K_7 = Exit loss coefficient for a type (o) fuel rod spacer flow cell

(8) K_8 = Exit loss coefficient for the fuel rod bundle at position 7-7

(9) K_9 = Exit loss coefficient for the fuel element at position 9-9

Reynolds Numbers

(1) R_x = Reynolds number for sodium flow in a central fuel rod bundle flow cell. This is away from a fuel rod spacer.

(2) R_c = Reynolds number for sodium flow in a type (c) fuel rod spacer flow cell

(3) R_d = Reynolds number for sodium flow in a type (d) fuel rod spacer flow cell

(4) R_o = Reynolds number for sodium flow in a type (o) fuel rod spacer flow cell

(5) R_s = Reynolds number based on the fuel rod spacer frontal dimension T_1

Miscellaneous

(1) n_1 = Number of fuel rods plus guide pins

(2) n_2 = Number of fuel rod spacers

(3) n_4 = Number of spacer or anchor bars

(4) n_5 = Constant accounting for the additional fuel element pressure loss due to fuel rod support fingers

(5) n_6 = Constant accounting for increase in friction factor due to misalignment of spacer strips forming flow cell walls

(6) n_7 = Constant to convert friction factors for aluminum cells to friction factors for stainless steel cells

(7) θ = Expansion angle of the fuel element nozzle between positions 2-2 and 3-3 (degrees)

(8) L = Reactor operating power level (MW_t)

(9) I = Equivalent number of average driver fuel elements

(10) ΔT = Sodium temperature rise, positions 1-1 to 9-9 (^{o}F)

(11) ρ = Average density of sodium between positions 1-1 and 9-9 (lb/ft^3)

(12) γ = Average specific weight of sodium between positions 1-1 and 9-9 (lb/ft^3)

(13) g = Gravitational constant = 32.2 lb-ft/lb-sec^2

(14) σ_1 = Free-flow area of the fuel rod bundle away from a fuel rod spacer, divided by the free-flow area of the fuel element between positions 3-3 and 4-4 or 7-7 and 9-9

(15) $\sigma_c = \sigma_d = \sigma_o$ = Free-flow area of a fuel rod spacer, divided by the free-flow area of the fuel rod bundle away from a fuel rod spacer

(16) Δp_{fuel} = Total fuel element pressure loss between positions 1-1 and 9-9 (psi)

FUEL ELEMENT ANNULUS HYDRAULICS

All position numbers refer to lines on the fuel element as exhibited in Figure 1.

Length

(1) L_3 = Length of the fuel element annulus, positions 6-6 to 8-8 (Figure 9) (ft)

(2) L_4 = Width of an annulus spiral channel (Figure 9) (in)

(3) L_5 = Length of an annulus spiral channel between positions 6-6 and 8-8 (Figure 9) (ft)

(4) T_5 = Diameter of an annulus spiral rib (Figure 2) (in)

Hydraulic Diameter

(1) D_{H_5} = Hydraulic diameter of a spiral channel (in)

Area

(1) A_5 = Total annulus flow area between positions 6-6 and 8-8 (in^2)

Velocity

(1) V_5 = Average sodium velocity in the spiral channels (fps)

Volumetric Flow Rate

(1) Q_5 = Volumetric flow rate of sodium through the annulus (ft^3/sec)

Friction Factor

(1) f_1 = Average Moody friction factor for a spiral channel

Loss Coefficients

(1) K_5 = Entrance loss coefficient for a spiral channel at position 6-6

(2) K_6 = Loss coefficient for bends in a spiral channel

(3) K_7 = Exit loss coefficient for a spiral channel at position 8-8

Reynolds Number

(1) R_5 = Reynolds number for sodium flow in a spiral channel

Miscellaneous

(1) n_1 = Number of bends per spiral channel between positions 6-6 and 8-8

(2) n_2 = Number of spiral ribs or channels in the annulus

(3) Θ = Spiral angle of an annulus channel (Figure 9) (degrees)

(4) ρ = Average density of sodium between positions 1-1 and 9-9 (lb/ft^3)

(5) γ = Average specific weight of sodium between positions 1-1 and 9-9 (lb/ft^3)

(6) g = Gravitational constant = 32.2 lb-ft/lb-sec^2

(7) Δp_{ann} = Annulus pressure loss between positions 6-6 and 8-8 (psi)

SODIUM LEAKAGE BETWEEN ANNULUS SPIRAL CHANNELS

All position numbers refer to lines on the fuel element as depicted in Figure 1.

Length

(1) L_1 = Clearance between annulus spiral ribs and the fuel element liner (in)

(2) L_5 = Length of the annulus spiral channels between positions 6-6 and 8-8 (Figure 9) (ft)

Area

(1) A_c = Flow area between adjacent spiral channels (ft^2)

Velocity

(1) M_c = Total sodium mass flow rate between adjacent spiral channels (lb/sec)

Miscellaneous

(1) n_1 = Number of turns per spiral channel between positions 6-6 and 8-8

(2) n_2 = Number of spiral ribs or channels in the annulus

(3) μ = Average viscosity of sodium between positions 1-1 and 9-9 (lb/ft-hr)

(4) g = Gravitational constant = 32.2 lb-ft/lb-sec^2

(5) Δp_{ann} = Annulus pressure loss between positions 6-6 and 8-8 (psi)

(6) Δp_c = Pressure differential across an annulus spiral rib (psi)

FUEL ROD SPACER STRENGTH

All position numbers refer to lines on the fuel element as illustrated in Figure 1.

Lengths

(1) L_6 = Width of strips forming a fuel rod spacer (Figures 2 and 10) (in)

(2) L_9 = Length of a fuel rod support finger (Figures 2 and 10) (in)

(3) L_{11} = Defined in Figures 2 and 10 (in)

(4) L_{13} = Width of a fuel rod support finger (Figures 2 and 10) (in)

(5) L_{14} = Length of the longest spacer strips (in)

(6) T_1 = Thickness of a spacer strip (Figures 2 and 10) (in)

Radius of Gyration

(1) r = Least radius of gyration of the spacer strip section indicated in Figure 10 (in)

Areas

(1) A_1 = Shear area defined by: $A_1 = 2(L_6-L_9)T_1$ (in^2)

(2) A_2 = Projected frontal area of a spacer strip (in^2)

(3) A_3 = Cross-sectional area (Figure 10) defined by the equation: $A_3 = (L_{11}-L_{13})T_1$ (in^2)

Velocity

(1) V_5 = Average sodium velocity in the fuel rod bundle between positions 6-6 and 7-7. This is away from a fuel rod spacer. (fps)

Coefficient of Drag

(1) C_d = Spacer strip drag coefficient

Forces

(1) F_1 = Drag force on the longest spacer strip (lb)

(2) F_2 = Drag force on a spacer strip section (Figure 10) (lb)

Miscellaneous

(1) n_2 = Coefficient accounting for end conditions of the spacer strip section (Figure 10)

(2) n_4 = Number of fuel rods supported by the longest spacer strip

(3) σ_g = Spacer strip shear stress (psi)

(4) S_y = Yield stress of 304 stainless steel (psi)

(5) E = Modulus of elasticity of 304 stainless steel (psi)

(6) Q = $\frac{S_y L_6^2}{n_2 \pi^2 E}$ (in^2)

(7) ρ = Average density of sodium between positions 1-1 and 9-9 (lb/ft^3)

(8) g = Gravitational constant = 32.2 lb-ft/lb-sec^2

ASSUMPTIONS

FUEL ROD BUNDLE HYDRAULICS

Lengths

(1) L_1 = 1.5 ft

(2) L_2 = 1.5 ft

(3) L_3 = 3.0 ft

(4) L_4 = 3.3 ft

(5) L_5 = 2.8 ft

(6) L_6 = 0.5 in.

(7) L_7 = 1.0 in.

(8) L_{10} = 1.98 in.

(9) L_{12} = 0.012 in.

(10) L_{13} = 0.030 in.

(11) L_c = 1.0 in.

(12) L_d = 0.5 in.

(13) L_o = 1.0 in.

(14) L_s = 1.0 in.

(15) L_t = 2.5 in.

(16) L_f = 0.5 in.

(17) L_g = 0.5 in.

(18) T_{l_c} = 0.015 in.

(19) T_{l_d} = 0.015 in.

(20) T_{l_o} = 0.015 in.

(21) T_{l_s} = 0.006 in.

(22) T_{l_t} = 0.006 in.

(23) T_2 = 0.080 in.

(24) T_4 = 0.125 in.

(25) P = 0.264 in.

Diameter

(1) D_r = 0.226 in.

Miscellaneous

(1) n_1 = 217

(2) n_2 = 6

(3) n_4 = 17

(4) n_5 = 1.1

(5) n_6 = 1.2

(6) n_7 = 1.2

(7) θ = 10 degrees

(8) L = 300 MW_t

(9) I = (equivalent number of average driver fuel elements) 53-1/2

(10) ΔT = 300°F

(11) ρ = 54.2 lb/ft^3

(12) γ = 54.2 lb/ft^3

FUEL ELEMENT ANNULUS HYDRAULICS

Length

(1) L_3 = 4.3 ft

Diameter

(1) T_5 = 0.050 in.

Miscellaneous

(1) n_1 = 9

(2) n_2 = 12

(3) θ = 67 degrees

(4) ρ = 54.2 lb/ft^3

(5) γ = 54.2 lb/ft^3

SODIUM LEAKAGE BETWEEN ANNULUS SPIRAL CHANNELS

Lengths

(1) L_1 = 0.001 in.

(2) L_5 = 4.3 ft

Miscellaneous

(1) n_1 = 1.5

(2) n_2 = 12

(3) μ = 0.79 lb/ft-hr

(4) Δp_{ann} = 70.0 psi

FUEL ROD SPACER STRENGTH

Lengths

(1) L_6 = 0.5 in.

(2) L_9 = 0.25 in.

(3) L_{13} = 0.03 in.

(4) T_1 = 0.015 in.

Velocity

(1) V_5 = 50.0 fps

Coefficient of Drag

(1) C_d = 2.0 Reference 2, Page 207, Table 5.1.

Miscellaneous

(1) n_2 = 0.25 Reference 8, Page 412

(2) n_4 = 17

(3) ρ = 54.2 lb/ft^3

(4) Fuel rod spacer material 304 stainless steel (S_y = 18,500 psi, 0.2% offset method, 1000°F; E = 19.2 x 10^6 psi, 1000°F). Reference 13, Page 569, Table 23.11.

APPENDIX

APPLICATION OF RESULTS

Results of this analysis have been applied to a parametric survey model, utilizing analog computer techniques to perform reactor design calculations.

The equation indicated on page 8 for determining fuel element pressure loss contains too many components for ease of use in the analog computer program. Therefore, values obtained from this equation (rectangular cell method) were employed to determine an effective entrance and exit loss and friction factor coefficient for a standard pipe flow pressure loss equation. The standard equation, indicated below, was then used on the analog computer for parametric analyses.

$$\Delta p_{fuel} = \frac{G^2}{2g\rho}\left[A + \frac{BL_5}{D_H}\left(\frac{GD_H}{\mu}\right)^{-0.2}\right]$$

Δp_{fuel} = Fuel element pressure loss

G = Mass velocity (sodium in the fuel element)

D_H = Hydraulic diameter of the fuel element including the fuel element liner (away from a fuel rod spacer)

L_5 = Length of the fuel rod bundle

A = Effective entrance and exit loss coefficient = 2.10

B = Effective friction factor coefficient = 0.888

ρ = Average sodium density between fuel element inlet and outlet

μ = Average sodium viscosity between fuel element inlet and outlet

g = Gravitational constant = 32.2 lb-ft/lb-sec^2

Values given for A and B relate to the cermet fuel design as analyzed in this report.

A subsequent study of oxide driver fuel element hydraulics for fuel rod spacers other than wire wrap, assumed for the oxide parameter survey, will result in an equation similar to that indicated above.

REFERENCES

1. D. P. Howlett, "Pressure Losses in Duct Systems: Part 1," Engineering Materials and Design, November, 1962.
2. D. P. Howlett, "Pressure Losses in Duct Systems: Part 2," Engineering Materials and Design, December, 1962.
3. Victor L. Streeter, Fluid Mechanics, Third Edition, McGraw-Hill, 1962.
4. A. N. de Stordeur, "Drag Coefficients for Fuel-Element Spacers," Nucleonics, June, 1961.
5. W. M. Kays and A. L. London, Compact Heat Exchangers, Second Edition, McGraw-Hill, 1964.
6. W. D. Weatherford Jr., John C. Tyler, and P. M. Ku, Properties of Inorganic Working Fluids and Coolants for Space Applications, WADC-59-598, December, 1959.
7. H. F. P. Purday, An Introduction to the Mechanics of Viscous Flow, Dover, 1949.
8. Erik Oberg and Franklin D. Jones (Ed.), Machinery's Handbook, Seventeenth Edition, the Industrial Press, 1964.
9. Theodore Baumeister (Ed.), Mechanical Engineers' Handbook, Sixth Edition, McGraw-Hill, 1958.
10. J. M. Davidson (Ed.), Progress Report, Conceptual Design, Fast Flux Test Facility, BNWL-CC-175, Volume 3, August, 1965.
11. W. M. Kays and A. L. London, "Heat-Transfer and Flow-Friction Characteristics of Some Compact Heat-Exchanger Surfaces, Part 1 - Test System and Procedure," ASME Translations, Volume 72, 1950.

12. D. C. Briggs and A. L. London, "The Heat Transfer and Flow Friction Characteristics of Five Offset Rectangular and Six Plain Triangular Plate-Fin Transfer Surfaces," Proceedings of the 1961-1962 International Heat Transfer Conference, ASME, 1963.

13. C. R. Tipton Jr. (Ed.), Reactor Handbook, Volume I, Second Edition, Interscience, 1960.